SCIENCE CHINA
Information Sciences

• REVIEW •

March 2026, Vol. 69, Iss. 3, 131401:1–131401:22
https://doi.org/10.1007/s11432-025-4662-3

Advances in material, structural, and integration strategies for DFB lasers in photonic sensing platforms

Miao HU[1,2], Tianyu ZHANG[1,2], Yao LI[1,2], Lei LIANG[1,3*], Li QIN[1,3], Yongyi CHEN[3,4*], Yue SONG[1,3], Yuxin LEI[1,3], Peng JIA[1,3], Cheng QIU[1,3], Yubing WANG[1,3], Chuantao ZHENG[5*] & Lijun WANG[1,3]

[1]*State Key Laboratory of Luminescence Science and Technology, Changchun Institute of Optics, Fine Mechanics and Physics, Chinese Academy of Sciences, Changchun 130033, China*
[2]*Daheng College, University of Chinese Academy of Sciences, Beijing 100049, China*
[3]*Jilin Changguang Jixin Technology Co., Ltd., Changchun 130022, China*
[4]*Jlight Semiconductor Technology Co., Ltd., Changchun 130102, China*
[5]*State Key Laboratory on Integrated Optoelectronics, College of Electronic Science and Engineering, Jilin University, Changchun 130012, China*

Received 28 May 2025/Revised 2 September 2025/Accepted 4 November 2025/Published online 14 January 2026

Abstract III-V-based distributed feedback (DFB) semiconductor lasers are fundamental building blocks for integrated photonic sensing because of their single-mode operation, narrow linewidth, and spectral coverage. This review provides a comprehensive overview of III-V DFB lasers, beginning with a comparison of major material platforms—GaN, GaAs, InP, GaSb, and quantum cascade laser (QCL) structures—across the visible to mid-infrared spectrum. We then highlight two main avenues of innovation: the use of quantum dot (QD) gain media for enhanced thermal robustness and spectral tunability, and the development of wavelength-specific DFB arrays and structurally integrated on-chip sources for compact, multichannel sensing. Building on these device-level innovations, we also review representative III-V-on-chip sensing systems that integrate DFB lasers with modulators, waveguides, and detectors on silicon or SiN platforms. These systems enable diverse applications in multi-gas spectroscopy, LIDAR, biochemical analysis, and quantum communication. Finally, we discuss the opportunities and challenges in achieving compact, low-power, and multifunctional sensing platforms through advanced integration and photonic system design.

Keywords DFB lasers, on-chip laser sources, photonic integration, III-V-on-silicon, optical sensing

Citation Hu M, Zhang T Y, Li Y, et al. Advances in material, structural, and integration strategies for DFB lasers in photonic sensing platforms. Sci China Inf Sci, 2026, 69(3): 131401, https://doi.org/10.1007/s11432-025-4662-3

1 Introduction

With the rapid advancement of integrated photonics and micro/nano-fabrication technologies, conventional macro-scale optical sensing systems are evolving toward highly integrated, low-power on-chip sensing platforms [1–3]. In diverse application scenarios, such as environmental monitoring, medical diagnostics, industrial control, and smart terminals, sensing solutions that offer high sensitivity, broad spectral coverage, high resolution, and scalable manufacturability are in demand. For instance, in early clinical screening, trace-level detection of molecular biomarkers imposes stringent requirements on the spectral resolution and stability of the light source [4]. Achieving multifunctional sensing with low power consumption has become a central challenge in system design, motivating research on advanced sensing architectures. Among various enabling components, lasers—particularly semiconductor lasers with narrow linewidth and precise tunability—are pivotal in determining overall system performance.

Spectroscopic sensing platforms rely on coordination among high-quality laser sources, gas cells, and sensitive photodetectors. Widely used techniques include tunable diode laser absorption spectroscopy (TDLAS), cavity ring-down spectroscopy (CRDS), surface-enhanced Raman scattering (SERS), and photoacoustic spectroscopy (PAS) [5–8]. These methods enable molecular identification at parts-per-billion (ppb) levels or lower and are applied to greenhouse gas monitoring, breath diagnostics, and chemical process control. By contrast, non-spectroscopic sensing modalities—such as optical phased array (OPA) LiDAR, interferometry, quantum key distribution (QKD), and biophotonic detection—impose equally stringent requirements on the coherence, modulation capability, and integration

* Corresponding author (email: liangl@ciomp.ac.cn, chenyy@ciomp.ac.cn, zhengchuantao@jlu.edu.cn)

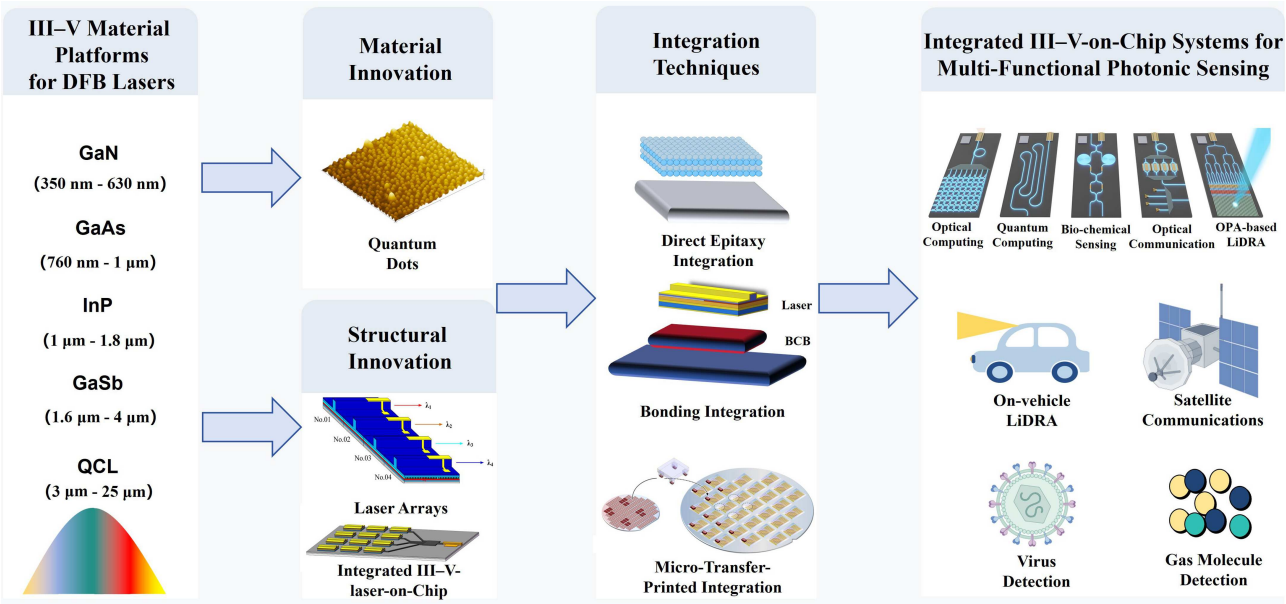

Figure 1 (Color online) Graphical overview of this review: III-V material platforms, structural innovations (e.g., QD DFBs and laser arrays), integration technologies (e.g., epitaxy, bonding, and micro-transfer-printing), and their system-level applications in spectroscopic sensing, LiDAR, quantum communication, and optical interconnects.

compatibility of the laser [9–11]. In this context, a high-quality and well-controlled light source is indispensable for realizing high-performance sensing systems.

III-V semiconductor lasers have emerged as the most promising light sources for integrated sensing platforms because of their compact footprint, low threshold current, high efficiency, electrical tunability, and compatibility with mainstream silicon photonics through various heterogeneous integration technologies [12, 13]. Among them, distributed feedback (DFB) lasers have gained widespread adoption because of their inherent single-mode operation, structural compactness, and excellent integrability. DFB lasers offer high side-mode suppression ratio (SMSR), narrow linewidth, and robust stability, making them indispensable in applications including spectroscopic sensing, communication, interferometry, and LiDAR [14,15]. Their emission wavelengths can be precisely engineered through tailored grating periods and waveguide designs, enabling wavelength-specific laser arrays supporting high power output, mid-infrared emission, and narrow-linewidth operation to accommodate various sensing platforms [16, 17].

As integration technologies continue to advance, III-V DFB lasers are evolving from discrete devices into arrayed light sources and integrated functional modules on a chip. To address the growing demand for high-performance mid-infrared light sources, novel active structures such as quantum dots (QDs), QCLs, and interband cascade lasers (ICLs) are increasingly adopted. These innovations have significantly extended the operation wavelength and thermal robustness of laser sources, accelerating the deployment and functional expansion of on-chip sensing systems in harsh environments.

In this review, we provide a systematic overview of the technological developments and integration strategies of III-V DFB lasers for sensing applications. We begin by surveying the latest progress in DFB laser performance across different spectral bands based on GaN, GaAs, InP, GaSb, and quantum cascade material systems, highlighting their respective optical properties and device optimizations as a foundation for future innovations. Subsequently, we review emerging gain media and structural innovations, focusing on quantum dot DFB lasers, DFB laser arrays, and chip-scale DFB sources enabled by epitaxial growth, wafer bonding, and micro-transfer-printing techniques. Finally, we explore the practical deployment and emerging trends of III-V-on-chip DFB lasers in representative on-chip sensing systems, including environmental monitoring, LiDAR, biochemical sensing, and quantum communication. We discuss their potential and challenges in building intelligent, multifunctional, and densely integrated photonic chips, offering analytical and practical guidance for next-generation sensing platform integration. A schematic overview of the review structure is illustrated in Figure 1, which outlines the materials, device innovations, and system-level integration approaches of III-V DFB lasers for multifunctional photonic sensing.

2 Material platforms for DFB lasers

To systematically present the material selection and structural characteristics of III-V DFB lasers across various spectral bands, this section begins with representative material platforms, including GaN, GaAs, InP, GaSb, and QCL systems. We analyze their gain characteristics, integration compatibility, and application adaptability, and highlight recent advances to signal upcoming directions.

III-V compound semiconductor lasers have emerged as a versatile platform covering the visible, near-infrared (NIR), mid-infrared (MIR), and far-infrared (FIR) regions because of their tunable band gaps, high gain efficiency, and excellent current injection capabilities. Among them, DFB lasers are pivotal for producing single-mode, narrow-linewidth, and highly stable light sources, which are critical in various high-precision sensing applications. The choice of substrate material fundamentally determines the operational wavelength and application scope: GaN-based platforms (350–630 nm) dominate the visible spectrum, thereby enabling uses including gas sensing, display technologies, and underwater optical communication [18,19]. GaAs-based platforms (760 nm–1 μm) and InP-based systems (1.0–1.8 μm) dominate the NIR regime, making them suitable for biomedical diagnostics, telecommunications, and on-chip photonic computing [20]. GaSb and its antimonide derivatives (1.6–4.0 μm) offer excellent bandgap engineering capabilities, positioning them as key platforms for MIR applications, including gas detection, molecular spectroscopy, and biomedical analysis [21–23]. Each material system exhibits distinct advantages in wavelength coverage, device performance, and integration potential, laying a robust foundation for the development of versatile, multi-application sensing platforms.

2.1 GaN-based DFB lasers

In the visible spectral region (400–700 nm), gallium nitride (GaN) and its related nitride alloys serve as a principal basis for DFB lasers. This is primarily explained by their wide bandgap, excellent thermal stability, and outstanding optoelectronic properties. Through engineering InGaN/GaN multiple quantum well (MQW) structures, efficient lasing can be achieved, covering a broad wavelength range from the near-ultraviolet to the red. In particular, blue (450 nm) and green (520 nm) devices have demonstrated remarkably high quantum efficiencies and low threshold currents, establishing GaN as the dominant approach for visible-wavelength semiconductor lasers [24,25]. Leveraging these advantages, GaN-based DFB lasers are now actively investigated across high-speed visible-light communication and sensing.

From a fabrication perspective, recent efforts have primarily focused on stress management and substrate engineering to enhance the quality and efficiency of InGaN/GaN MQWs. For example, introducing graphene as a buffer layer mitigates biaxial stress in GaN thin films, thereby improving indium incorporation and leading to a redshift in the emission wavelength [26]. Moreover, metal-modulated molecular beam epitaxy (MBE) permits the manufacture of high-quality cubic InGaN/GaN MQWs with superior interfacial smoothness and optical performance compared to conventional methods [27]. Growth on semi-polar GaN substrates additionally reduces the quantum-confined Stark effect (QCSE), significantly improving the emission efficiency in the green spectral region [28]. Another significant milestone is the direct growth of InGaN/GaN MQW structures on silicon substrates, thereby enabling room-temperature continuous-wave electrically pumped blue laser diodes with a threshold current density as low as 7.8 kA/cm^2 [29]. This breakthrough reduces fabrication costs and widens opportunities for visible-light integration on silicon photonics platforms. Additionally, InGaN/GaN quantum dot structures, because of their strong carrier localization effects, have demonstrated great promise for improving both conversion efficiency and response speed [30].

For applications, GaN-based DFB lasers have demonstrated considerable potential in visible-light communication (VLC) and underwater wireless optical communication (UWOC). In free-space VLC systems, GaN lasers have achieved data transmission rates as high as 4 Gbps [31]. DFB InGaN laser diodes operating at 480 nm have demonstrated a high SMSR of 42.4 dB, an optical power of approximately 14 mW, and a resolution-limited linewidth of 34 pm under continuous-wave operation, enabling VLC data rates up to 10.5 Gbps [32]. In UWOC, green GaN laser diodes achieved 2.70 Gbps over a 34.5 m transmission distance [33], whereas 450 nm GaN-based UWOC systems realized 50 Mbps over a 3 m link with a bit error rate below the forward error correction threshold [34]. Furthermore, UWOC systems based on GaN micro-LED arrays demonstrate the feasibility of achieving high data rates and long transmission distances [18,35].

Overall, GaN-based DFB lasers are prominent in the III-V semiconductor laser family, primarily operating in the visible-light spectrum. With their wide bandgap, high thermal stability, and excellent optoelectronic properties, GaN lasers serve as dependable sources for applications such as visible-light optical sensing, high-speed optical communication, and underwater optical communication.

2.2 GaAs- and InP-based DFB lasers

In the NIR range (0.8–2 μm), III-V material platforms represented by GaAs and InP play a pivotal role in DFB laser design because of their mature epitaxial growth processes and excellent optoelectronic properties. These platforms are widely adopted in fields such as optical communication and sensing. Recent studies report notable advances in structural design and performance optimization. For instance, surface-emitting DFB lasers incorporating second-order gratings and phase shifts have demonstrated stable single-mode operation with data transmission rates as high as 24 Gb/s, maintaining lasing performance over a wide temperature range [36]. Additionally, uncooled DFB lasers featuring trench-embedded waveguide structures exhibit high-speed direct modulation capabilities with a bandwidth of 15.3 GHz at 85°C, offering a low-cost and highly integrated solution for data centers and fronthaul communication applications [37].

With continuous improvements in device performance, GaAs and InP platforms record notable gains in epitaxial integration. For example, selective area growth (SAG) has enabled monocrystalline GaAs nanowires on silicon substrates, thereby reducing lattice mismatch-induced defects [38]. Similarly, the self-catalyzed growth of InP nanowires improves material processability and integration flexibility [39]. Moreover, in fields such as biosensing and infrared spectroscopy, GaAs waveguides with high optical nonlinearity and enhanced photoluminescence properties show considerable promise in trace-level detection tasks such as DNA analysis [40–42].

Overall, GaAs- and InP-based DFB lasers have established a solid foundation for application in high-speed communication, biomedical detection, and near-infrared sensing. Their continued structural innovations and technological maturity provide a reliable path for integrating III-V lasers onto silicon photonic platforms.

2.3 GaSb-based DFB lasers

The MIR spectral range (2–20 μm) is increasingly required for environmental monitoring, biomedical diagnostics, and industrial sensing. GaSb and its derivative antimonide materials are central bases for DFB lasers in this region owing to their excellent bandgap tunability and thermal stability. Using InGaAsSb quaternary alloys to engineer MQW structures, GaSb-based DFB lasers deliver continuous-wave emission across the 2.1–4.3 μm band. Device performance—including output power and thermal tuning characteristics—can be further enhanced through strain-compensated growth and optimized sidewall grating schemes [43, 44].

Structurally, the laterally coupled distributed feedback (LC-DFB) architecture—featuring metal-loaded surface gratings—has become a mainstream approach for achieving single-mode operation. Chinese teams have demonstrated GaSb-based LC-DFB lasers with Cr metal gratings, achieving a center wavelength of 2004 nm, an output power of 2 mW, and an SMSR exceeding 30 dB, suitable for CO_2 detection scenarios [45, 46]. Moreover, photonic crystal structures have been introduced to improve mode selectivity, in which adjusting the displacement and etch depth of dual-hole lattice geometries leads to improved threshold characteristics and emission stability [47–49]. In practical sensing, GaSb-based DFB lasers have been tuned to match absorption lines of molecules such as CO_2 and N_2O. For example, Mide Technologies has developed DFB emitters with center wavelengths near 2.0 μm and 2128 nm, aligning with CO_2 and N_2O absorption peaks, and achieving SMSRs of 35.59 and 36.7 dB, respectively—demonstrating strong potential for trace gas analysis [50].

Despite their promising MIR performance, GaSb-based DFB lasers remain challenged to attain high-temperature stability, robust single-mode operation, and scalable manufacturing. Current research centers on improving strain-balanced MQW designs, hybrid grating configurations, and feedback stabilization techniques to expand their utility in MIR sensing systems.

2.4 DFB quantum cascade lasers

QCLs are unipolar semiconductor devices that rely on intersubband transitions within coupled quantum wells, in contrast with conventional bipolar lasers that operate via interband recombination. Compared to ICLs, QCLs achieve photon emission through engineered electron tunneling between quantized subbands, enabling a broad spectral span [51, 52]. To date, QCLs show continuous-wave and pulsed operation from 3 to 25 μm and across the 1–6 THz range, making them highly attractive for trace gas sensing, infrared imaging, and free-space communications [53–55]. The introduction of DFB gratings into QCL structures enables precise mode selection and stable single-mode output, vital to high-resolution spectroscopy and spectrally selective sensing systems [56–59].

In recent years, DFB-QCL design has increasingly employed machine-learning-assisted optimization strategies. For example, Tang et al. [60] applied a neural network-based multilayer perceptron (MLP) model to predict resonant modes in terahertz QCLs, improving mode control and fabrication tolerance. A schematic of the DFB-QCL design applied to sampled convolutional neural networks with an MLP architecture is depicted in Figure 2. Furthermore,

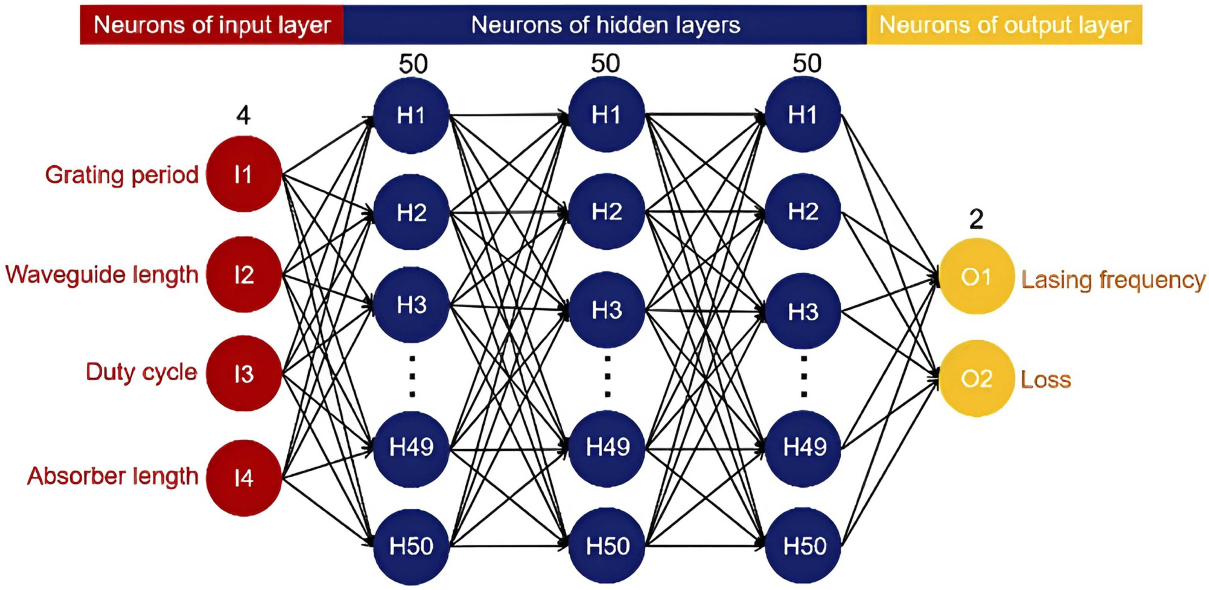

Figure 2 (Color online) DFB-QCL design based on sampled convolutional neural networks with MLP architecture [60].

the Hashimoto group introduced a high-gain vertical transition structure, achieving a 0.93 W output power with low threshold current and an SMSR greater than 25 dB [61]. Sampled grating designs have also been extensively used to balance single-mode selectivity and optical power output [62].

Additionally, DFB-QCLs integrate well with high-sensitivity techniques such as cavity ring-down spectroscopy (CRDS) and PAS to achieve trace gas detection at the parts per billion by volume (ppbv) level [63–66]. For instance, Gadedjisso-Tossou et al. [67] demonstrated the detection of NH_3 using a pulsed DFB-QCL source at 6.8 μm, achieving a sensitivity of 9 ppbv within 120 s using CRDS. Similarly, Murata et al. [68] built a compact 7 μm DFB-QCL that operates reliably under low power, making it suitable for portable methane detection platforms.

In summary, DFB-QCLs fabricated on GaSb substrates significantly broaden the spectral bandwidth and application domains of III-V semiconductor lasers in the mid-infrared. With continued advances in bandgap engineering, grating design, and heterogeneous integration, DFB-QCLs are increasingly vital to high-resolution, multiband spectroscopic sensing platforms. The following section will explore the frontier developments of DFB lasers based on novel gain media—such as quantum dot lasers—and their arrayed and on-chip integrated configurations for multifunctional sensing systems.

3 Technical advancements in DFB lasers

3.1 Quantum dot DFB lasers

Amid rising demand for high-performance laser sources in applications such as precision gas sensing, environmental monitoring, and industrial process control, conventional DFB lasers based on strained quantum wells (QWs) are increasingly encountering performance bottlenecks, especially in terms of wavelength selectivity, thermal stability, and integration compatibility. Against this backdrop, QDs, as zero-dimensional nanostructures with 3D carrier confinement, have attracted significant attention in the design of active regions for semiconductor lasers owing to their unique density of states and carrier confinement characteristics [69–72]. Relative to conventional QW-based devices, QD lasers offer lower threshold currents, superior temperature stability, narrower gain spectra, and greater design flexibility in emission wavelengths, making them highly suitable for applications in sensitive gas detection and compact on-chip monitoring systems [73–75].

Integrating QDs into DFB laser structures enhances single-mode selectivity and wavelength stability and robustly suppresses thermal drift and mode hopping. These advantages are especially beneficial for long-term stable operation in harsh environments, such as those encountered in spectroscopic sensing and chip-scale photonic sensing platforms [76–78]. DFB lasers employing QDs have now been demonstrated across various III-V material systems (e.g., InAs/InGaAs and GaSb-based QDs), with emission wavelengths extending from 3 to 5 μm, thus covering key absorption bands of CO, CH_4, NH_3, and other gases [79–82].

On the GaN material platform, QD structures offer notable performance benefits for visible-light lasers and optoelectronic devices. Relative to conventional quantum well devices, GaN/InGaN QD lasers exhibit stronger carrier localization, leading to enhanced optical performance. In microdisk laser configurations, GaN/AlN QDs demonstrate extremely high quality factors (Q-factors), reflecting the low-loss characteristics of the optical cavity [83]. Additionally, InGaN/GaN QDs in photodetectors leverage polarization-induced barriers and single-carrier superlattice structures to achieve high gain and excellent wavelength selectivity while reducing dark current and enhancing amplification [84]. In light-emitting diode (LED) devices, QD structures enable more uniform carrier distribution, lowering the carrier density within individual dots, effectively suppressing Auger recombination losses, and thereby improving device efficiency and reducing turn-on voltage [85].

On the GaAs platform, InAs/GaAs QD structures substantially enhance modal stability and thermal tolerance. For instance, a microdisk laser based on this system exhibited low threshold current and robust single-mode emission in the near- to mid-infrared spectral range [80]. Xu et al. [81] reported an InAs/GaAs quantum dot (QD) laser grown on a GaAs/Ge/Si virtual substrate, highlighting the potential of monolithic integration on silicon. The device employs a separate-confinement heterostructure (SCH) design with five stacks of InAs dot-in-well (DWELL) active layers embedded within GaAs/AlGaAs waveguides, which provide strong carrier and optical confinement, as shown in Figure 3(a). Atomic force microscopy (AFM) measurements of uncapped InAs QDs reveal an average lateral size of approximately 30 nm and a density of $\sim 5.6 \times 10^{10}$ cm^{-2}, indicating a uniform distribution of dots across the surface (Figure 3(b)). Such high-quality morphology directly supports the excellent device performance, including a lasing wavelength of 1320 nm, output power of 153 mW under continuous-wave operation, and stable functionality up to 80°C, thereby confirming the strong thermal robustness of the QD laser.

In the InP-based material system, InAs/InP QD structures exhibit high modal gain and efficient long-wavelength emission, enabling the development of broadband tunable DFB sources [79]. Additionally, GaSb/InGaAs QDs grown on InP substrates have been explored for building high-performance QD infrared photodetectors and optoelectronic integration devices [82]. On silicon platforms, Kwoen et al. [86] demonstrated the robust epitaxial growth of InAs/GaAs QDs on on-axis Si (001) substrates using a GaAs buffer layer. This approach enables high-temperature continuous-wave (CW) operation above 100°C while mitigating challenges such as thermal stress and dislocation generation in heterogeneous integration. During device fabrication, 7 μm-wide laser mesas were formed via photolithography and wet etching, and AuGeNi/Au contacts were deposited on the p- and n-type layers. The devices were cleaved to a length of 1.1 mm, with no high-reflectivity coatings applied to the facets. AFM of the uncapped QDs indicates an average lateral size of approximately 30 nm and a density of 5×10^{10} cm^{-2}, as shown in Figures 3(c) and (d), demonstrating uniform size and dense arrangement. Despite the relatively high threading dislocation density (TDD) in the GaAs buffer layer and the absence of modulation p-doping, the fabricated QD lasers exhibit robust high-temperature performance, confirming their potential for integration into silicon CMOS technology.

In summary, the integration of QDs into DFB lasers expands the performance boundaries at the material level and significantly improves device-level capabilities in terms of integration, wavelength control, and environmental resilience. With continued progress in III-V/Si heterogeneous integration technologies, quantum-dot-based DFB lasers are expected to become pivotal components in high-performance, tunable, and broadband photonic platforms.

3.2 III-V laser source integration

3.2.1 *DFB laser arrays*

With increasing demands across multispecies, broadband, and multi-scenario sensing applications—including gas detection, biochemical sensing, environmental monitoring, and LiDAR. DFB lasers operating at a single wavelength fail to satisfy the requirements of complex photonic sensing systems. Consequently, one of the key development directions for integrated laser sources is the construction of DFB laser arrays capable of multi-wavelength emission. These arrays fall into discrete and monolithically integrated forms, enabling either chip-level hybrid assembly or on-chip multi-grating fabrication to achieve both high integration density and broad spectral coverage. Such configurations provide a robust basis for next-generation high-performance spectroscopic and sensing platforms [87, 88].

Discrete DFB laser arrays. Discrete DFB arrays typically consist of multiple individually packaged DFB lasers, which can readily match the absorption peaks of various gas species. Leveraging time-division multiplexing (TDM) or frequency-division multiplexing (FDM) techniques, these arrays support parallel multichannel detection with high wavelength tuning flexibility and simplified thermal management—making them ideal for rapid deployment of prototype sensing systems. For instance, Wang et al. [89] reported a gas sensor system based on quartz-enhanced photoacoustic spectroscopy (QEPAS) using two DFB lasers and TDM, enabling simultaneous

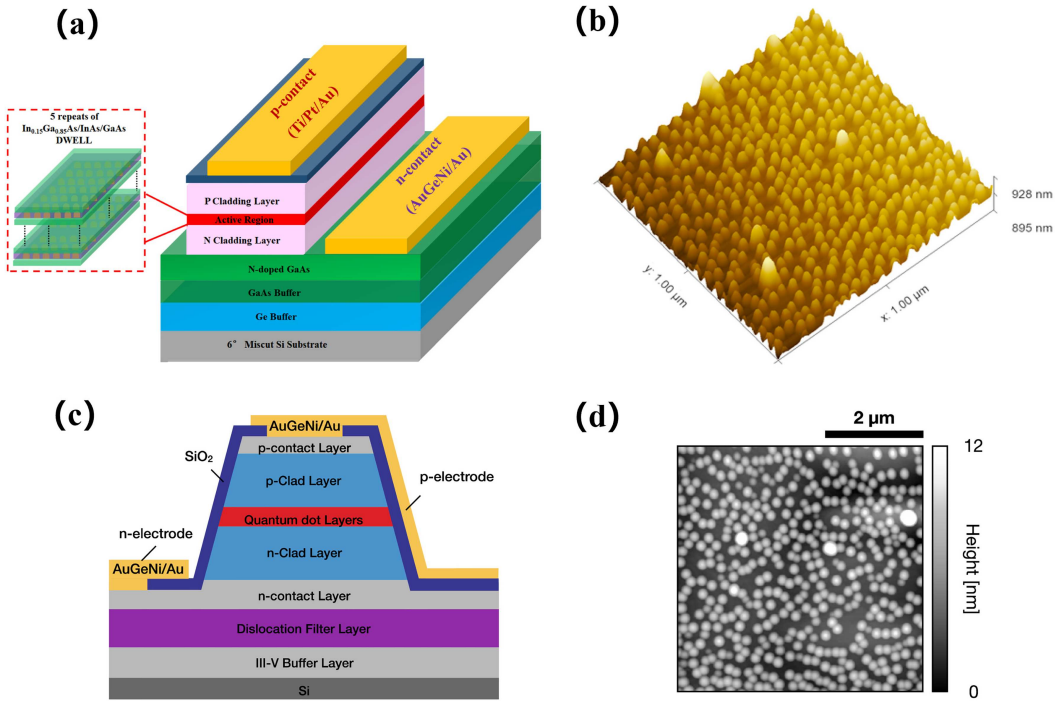

Figure 3 (Color online) (a) Schematic of an InAs/GaAs QD laser structure; (b) AFM image of uncapped InAs QDs (1 μm × 1 μm) [81]; (c) device structure schematic of an InAs/GaAs QD laser on an on-axis Si(001) substrate; (d) AFM image of InAs/GaAs QDs on a GaAs buffer layer on on-axis Si(001) [86].

detection of dual gas species. Jiang et al. [90] used four DFB lasers for the identification of a gas mixture containing CH_4, C_2H_2, C_2H_4, and C_2H_6. Moreover, Zou et al. [91] integrated five different-wavelength DFB lasers with frequency-modulated TDM (F-TDM) and wavelength modulation spectroscopy (WMS) to achieve high-precision detection of six gases, including CH_4, C_2H_6, C_2H_2, C_2H_4, CO, and CO_2.

To enhance the spectral coherence of discrete laser arrays, several linewidth-narrowing techniques are employed, including Rayleigh backscattering feedback, self-injection locking, and dual-cavity feedback schemes. Li et al. [92] used a 30-m high-numerical-aperture fiber (HNAF) to induce Rayleigh backscattering for simultaneous linewidth compression across four different-wavelength DFB lasers, reducing the linewidth from MHz to kHz scale. The four butterfly-packaged DFB lasers (LD1–LD4) are combined via a multiplexer with 0.8 nm channel spacing. The standard port of the multiplexer is split by a 3 dB coupler into two paths: one sent toward an optical spectrum analyzer through an isolator to suppress reflections, and the other routed into a second 3 dB coupler. One output of the second coupler drives a demultiplexer that separates the four wavelengths into individual channels (CH1–CH4). Meanwhile, the other output is sent through the HNAF, where Rayleigh backscattering provides feedback into the laser cavities. End-facet reflections of the HNAF are suppressed via angled polishing and coiling, ensuring that Rayleigh backscattering is the primary feedback source. This configuration enables simultaneous linewidth narrowing across all four DFB lasers.

In another approach, multiple DFB lasers were simultaneously self-injection-locked to a single high-Q microring resonator, achieving white frequency noise suppression by more than 40 dB [93]. The four butterfly-packaged DFB lasers are connected through a multiplexer and optical circulator to a microring resonator, which provides resonant feedback via evanescent coupling. The lasers exhibit instantaneous linewidths compressed to the Hz level and deliver 1.7–3.3 mW per channel. Non-degenerate four-wave mixing between the locked lasers generates additional frequency comb lines, showing a scalable on-chip approach for coherent multi-wavelength sources. Lan et al. [94] introduced a dual-cavity feedback structure in a DFB array, where inter-cavity interference effectively suppressed side modes and reduced the linewidth to approximately 800 Hz while maintaining an SMSR above 40 dB. This approach offers a scalable solution for large-scale on-chip wavelength-division multiplexing (WDM) sensing networks.

In summary, discrete DFB laser arrays, by leveraging multiple coordinated sources and external cavity feedback mechanisms, substantially expand spectral coverage and improve linewidth control, demonstrating broad applicability in multi-gas and high-resolution sensing scenarios. However, the bulky packaging and greater system complexity of such arrays limit their suitability for compact, highly integrated platforms. These constraints have fueled the rapid advancement of monolithically integrated DFB arrays, which offer improved scalability and integration density,

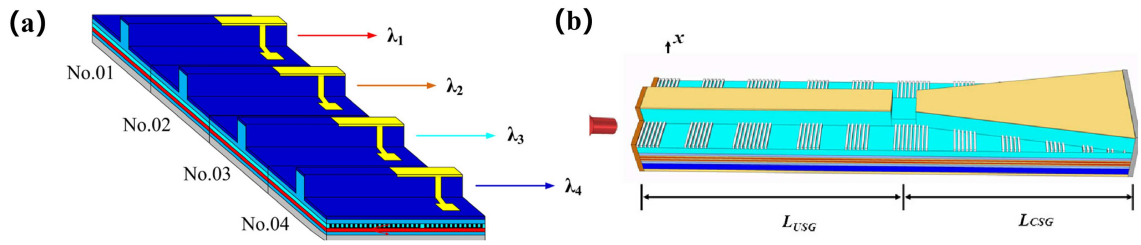

Figure 4 (Color online) (a) The REC-GR-DFB laser array [97]; (b) dual-section DFB laser with three-equivalent-phase-shift design [101].

a significant trend in the evolution of integrated laser sources.

Integrated DFB laser arrays. Compared with discrete DFB laser arrays, monolithically integrated DFB laser arrays offer substantial advantages in integration density, stability, and manufacturing consistency. By incorporating different grating periods or grating designs on a single chip, multi-wavelength outputs are realized while substantially simplifying the packaging process. For example, Sun et al. [95] demonstrated a DFB laser array based on a four-phase-shift sampled Bragg grating (4PS-SBG), which realized a wavelength spacing of 0.8 ± 0.026 nm, single-channel output power of up to 33 mW, and an SMSR greater than 50 dB. The design utilized sidewall Bragg grating ridge waveguides and required only a single metal-organic vapor phase epitaxy (MOVPE) growth and etching step, significantly improving fabrication yield. This structure fits dense wavelength division multiplexing (DWDM) systems and integrated photonic sensing chips.

In recent years, the reconstructed equivalent chirp (REC) technique has been commonly used to improve wavelength uniformity and fabrication reproducibility in DFB laser arrays [96, 97]. As shown in Figure 4(a), each REC-GR-DFB laser consists of a 450 μm active DFB section and a 500 μm grating reflector (GR) section, fabricated on an n-InP substrate with a multi-quantum-well InAlGaAs epitaxial structure. Sampled gratings are formed via holographic exposure and photolithography, and ridge waveguide processing with p-metal contacts ensures electrical injection. Additionally, a small etched region between the DFB and GR sections enhances isolation. Anti-reflection coatings are applied to both facets, resulting in improved slope efficiency, SMSR, and threshold current. Chen et al. [98] proposed a REC-based array with a tuning range of 1650.4–1657.6 nm, covering absorption bands of CH_4, H_2O, CO_2, and CO. Yuan et al. [99] developed a REC array with 100 GHz channel spacing, SMSR exceeding 48 dB, and a modulation bandwidth of over 13 GHz at a bias current of 100 mA. To further improve array consistency, Tang et al. [100] combined sampled Bragg grating (SBG) with the REC method and used single-step electron beam lithography (EBL) to fabricate high-uniformity arrays while suppressing zero-order reflections, making them suitable for large-scale DFB array manufacturing. Additionally, a high-power tapered dual-section DFB laser structure based on REC was reported, incorporating a three-equivalent-phase-shift (3EPS) design and tapered waveguides. This device achieved a maximum output power of 306.5 mW and SMSR exceeding 40 dB [101]. As illustrated in Figure 4(b), the laser consists of a uniform waveguide section of approximately 400 μm to ensure fundamental transverse mode operation and a tapered waveguide section of about 600 μm that expands the mode field and increases the gain area, thereby reducing optical power density and enabling higher output power. Furthermore, HR/AR facet coatings are applied to enhance power extraction and device performance.

In summary, structurally integrated DFB laser arrays—whether discrete or monolithic—demonstrate substantial advantages in multi-wavelength coverage, consistency, and high-density integration. With the adoption of external cavity feedback, self-injection locking, and REC grating technologies, laser arrays now exhibit superior linewidth compression and application scalability, positioning them as promising multichannel sources for multi-species gas detection and high-speed optical communication.

On this basis, recent research has further explored how to implement on-chip DFB light sources using unified fabrication processes such as epitaxy, wafer bonding, and micro-transfer-printing. The following section will focus on these integration techniques and their roles in enabling high-performance, tunable on-chip DFB lasers.

3.2.2 *Integrated III-V-laser-on-chip*

Conventional gas optical sensing systems typically rely on discrete laser diodes, complex free-space optical coupling, and high-precision external detection modules. This architecture is bulky, expensive, and highly sensitive to environmental vibrations and temperature fluctuations, making it unsuitable for scenarios such as industrial field monitoring, emergency environmental detection, and portable applications. Although monolithic integration of laser arrays has made significant strides in system miniaturization, most approaches remain limited to the light source alone, lacking the functional diversity and integration density required by advanced multimodal sensing

systems [102–104].

To address this limitation, recent efforts prioritize integrating III-V lasers, optical waveguides, modulators, photodetectors, and other critical photonic components onto a single chip. Leveraging silicon photonics as the foundational platform, these systems target high-performance, compact, and multifunctional on-chip sensing capabilities [105–110]. From a fabrication standpoint, current mainstream approaches for integrating III-V light sources onto silicon platforms fall into four process-driven strategies: direct epitaxy, adhesive bonding, micro-transfer-printing, and chip-scale packaging. The following section highlights recent advances in on-chip laser sources and their integration into photonic sensing systems, with an emphasis on fabrication methodologies.

Epitaxy integration. Direct epitaxial growth permits integration of III-V active layers directly onto silicon substrates, offering a compact form factor, efficient mode coupling, and favorable thermal compatibility—critical for high-density on-chip integration. However, significant challenges remain owing to the lattice constant and thermal expansion mismatches between III-V materials and silicon. These mismatches often induce threading dislocations, antiphase domains, and other structural defects that degrade device performance and reliability [111, 112]. In this context, quantum dot (QD) structures, owing to their high tolerance to crystalline defects, offer a promising route to enhance the robustness of epitaxial lasers [113].

In 2015, Wang et al. [114] reported a DFB laser array fabricated via selective epitaxial growth on silicon, achieving a center wavelength of 930.5 nm and an output power of up to 6.4 mW. The platform enabled butt-coupling between III-V lasers and planar silicon waveguides, providing a viable pathway for scalable laser array integration. The schematic of the monolithic integrated InP DFB laser on silicon is shown in Figure 5(a). Each laser consists of a high-quality InP waveguide with first-order gratings, including a $\lambda/4$ phase shift section at the center. To facilitate vertical light extraction for characterization, second-order gratings are located 30 μm away from the DFB cavity. The differently colored output gratings illustrate the tunable lasing wavelengths of the device.

Another study reported an organic-inorganic hybrid DFB laser fabricated using inkjet printing on a silicon nitride waveguide platform. Using organic gain media, this device achieved visible-wavelength lasing while maintaining low-cost, CMOS-compatible fabrication—making it suitable for low-power sensing applications [115]. Figure 5(b) depicts the geometry of the silicon nitride organic hybrid (SiNOH) DFB laser: the dye-doped polymer gain layer was deposited into an opening of the SiO_2 cladding by inkjet printing, enabling localized and flexible processing. The laser operates at 630 nm and injects light into a tapered Si_3N_4 waveguide to ensure single-mode output. Additionally, an S-bend structure with lateral offset routes the optical signal to the chip facet for fiber coupling, thereby suppressing background light from unguided modes.

Wang et al. [116] further advanced the field by integrating InAs/GaAs quantum dot gain layers onto silicon substrates to realize a QD-DFB laser array with a 100 nm wavelength coverage. The device exhibited single-mode lasing centered around 1300 nm with a high SMSR of 50 dB, suitable for DWDM systems. Figure 5(c) presents a cutaway schematic of the silicon-integrated DFB laser array, showing the vertical layer structure, the ridge waveguides, and the output coupler (not to scale). This schematic highlights the vertical integration and arrangement of the quantum dot active region, clarifying the device configuration for stable single-mode operation and efficient optical confinement.

To enable multiwavelength output on a single chip, Karnik et al. [103] constructed a DFB QCL array directly on silicon using molecular beam epitaxy (MBE). Each laser ridge was 9.5 μm wide with 300 μm separation, and the five lasers were arranged in a master oscillator-power amplifier (MOPA) configuration, covering the 4.58–4.71 μm spectral range. Figure 5(d) depicts the WBC QCL array integrated with the AWG and cone output amplifiers, highlighting the vertical layer structure, the gain medium region, and the coupling configuration between the DFB lasers and waveguides. The AWG channels are aligned with the emission wavelengths of the corresponding DFB lasers, and an output amplifier amplifies the combined signal.

Additionally, the feasibility of selectively growing InAs-, InSb-, and GaSb-based lasers on silicon is under study, along with their integration onto SiN waveguides [12, 117, 118]. In terms of thermal management, the epitaxial integration of QD lasers on high thermal conductivity substrates such as silicon carbide has shown improved thermal robustness and output characteristics under elevated temperatures [119].

Bonding integration. Bonding-based integration facilitates coupling of III-V semiconductor materials with silicon photonic platforms by physically combining the active gain region with passive waveguide circuits. This process offers high coupling efficiency, compact form, and strong compatibility with complementary metal-oxide-semiconductor (CMOS) fabrication. Among various approaches, wafer bonding offers a wafer-scale route for achieving consistent performance with good scalability and cost-effectiveness [120–123].

Wang et al. [124] developed a four-channel distributed feedback quantum cascade laser (DFB-QCL) array with a tuning range of 2.28–2.43 μm, based on a silicon photonic integration platform. The DFB-QCL array was realized through bonding-based fabrication techniques, achieving a continuous tuning range of 10 nm and an SMSR of

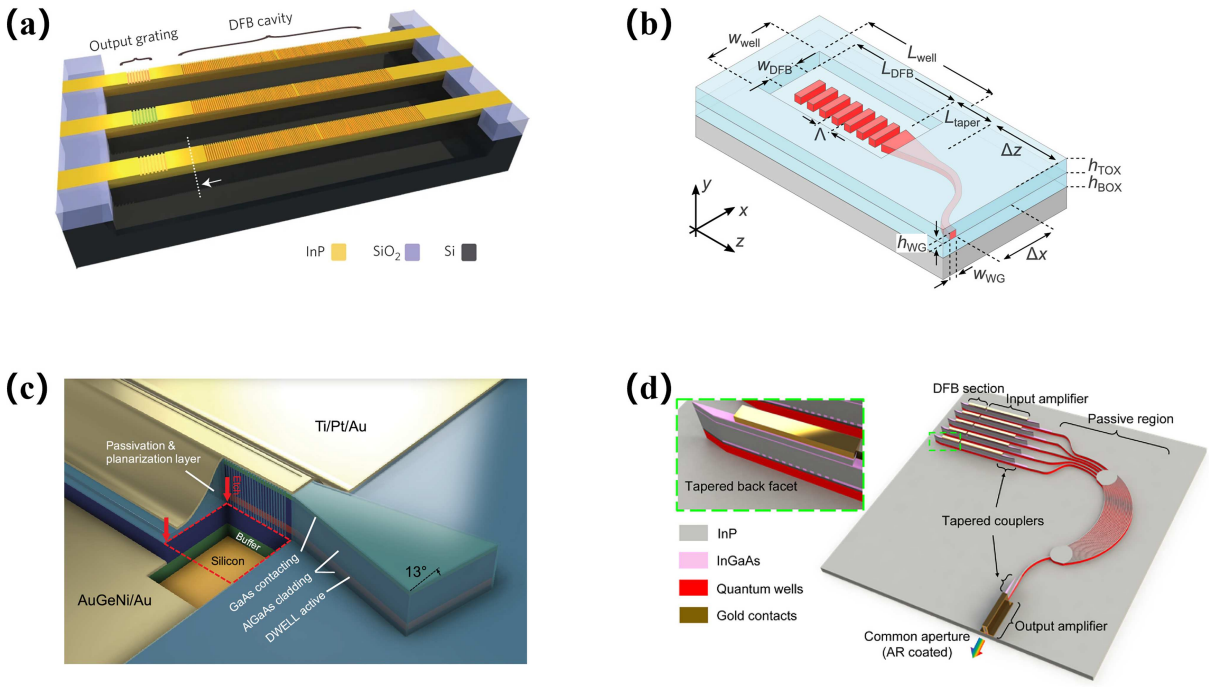

Figure 5 (Color online) (a) Schematic of monolithically integrated InP DFB lasers on Si [114]; (b) geometry of SiNOH DFB laser with waveguide taper for single-mode output [115]; (c) cross-section view of a silicon-integrated DFB laser array [116]; (d) schematic of WBC QCL array integrated with AWG and tapered output amplifier [103].

40 dB in the MIR regime, demonstrating strong potential for mid-IR photonic applications.

Stankovic et al. [125] reported a 1310 nm III-V/Si DFB laser using a top-etched grating in the silicon waveguide to provide feedback. The device achieved single-mode emission with a continuous-wave output power of ∼2.1 mW at room temperature and an SMSR of 45 dB, confirming its stable operation and good integration characteristics.

Keyvaninia et al. [126] employed a divinylsiloxane-benzocyclobutene (DVS-BCB) adhesive process in a die-to-wafer configuration to integrate III-V active materials with a silicon photonics platform. The resulting 1550 nm DFB laser exhibited a narrow linewidth of 1 MHz, a high SMSR of 50 dB, and an output power of 14 mW at 10°C, maintaining stable performance up to 60°C, indicating excellent thermal reliability and potential for system-level integration. As shown in Figure 6(a), the device features the III-V mesa bonded to the silicon waveguide via a 35 nm DVS-BCB adhesive layer, a spot-size converter for efficient mode transfer from the III-V laser to a 400 nm silicon waveguide, and a second spot-size converter transitioning the mode to a 220 nm strip waveguide, ensuring robust single-mode operation across the hybrid platform.

Thiessen et al. [127] proposed a "back-side-on-buried oxide" (BSoBOX) integration scheme, wherein III-V materials are bonded to the back side of a silicon photonic chip. This architecture supports multilayer silicon photonics and enhances fabrication flexibility. The resulting DFB lasers delivered stable single-mode emission from 20°C to 60°C, with up to 15 mW output power and ∼50 dB SMSR, making them suitable for advanced on-chip system expansion.

In another approach, Chowdhury et al. [128] demonstrated photonic wire bonding (PWB) to create three-dimensional interconnects between commercial DFB lasers and multi-channel passive silicon photonic circuits. The DFB laser was placed in a pre-etched deep trench on the silicon chip using solder-based die bonding. The PWB structure, fabricated via femtosecond laser-written polymer waveguides, supports up to 30 μm alignment tolerance and achieves insertion losses as low as 0.73 ± 0.15 dB. As shown in Figure 6(b), the PWB waveguide follows a tapered path from the laser facet to the silicon surface coupler, reducing mode mismatch and back-reflections. The process integrates laser placement, 3D interconnect formation, and polymer waveguide curing in a compact workflow, providing a flexible and reproducible route for hybrid on-chip integration.

In the context of quantum light sources, QD lasers—known for their low threshold current and strong temperature stability—have been successfully merged with silicon photonic platforms through bonding techniques. Using large-area bonding, InP waveguides embedded with InAs QDs were bonded with silicon-on-insulator (SOI) substrates to form on-chip QD lasers. These lasers exhibit single-mode emission at telecom wavelengths under electrical injection with ultralow threshold current densities, highlighting their strong compatibility and potential in quantum

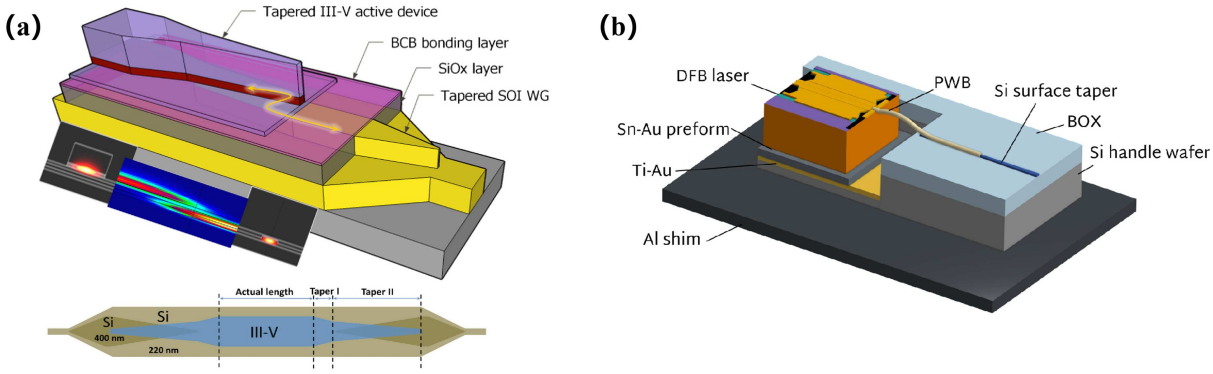

Figure 6 (Color online) (a) Three-dimensional schematic of the DVS-BCB bonded III-V-on-silicon DFB laser with spot-size converter [126]; (b) chip schematic showing tin-gold bonded DFB laser with photonic wire bond connecting the laser facet to the silicon surface coupler [128].

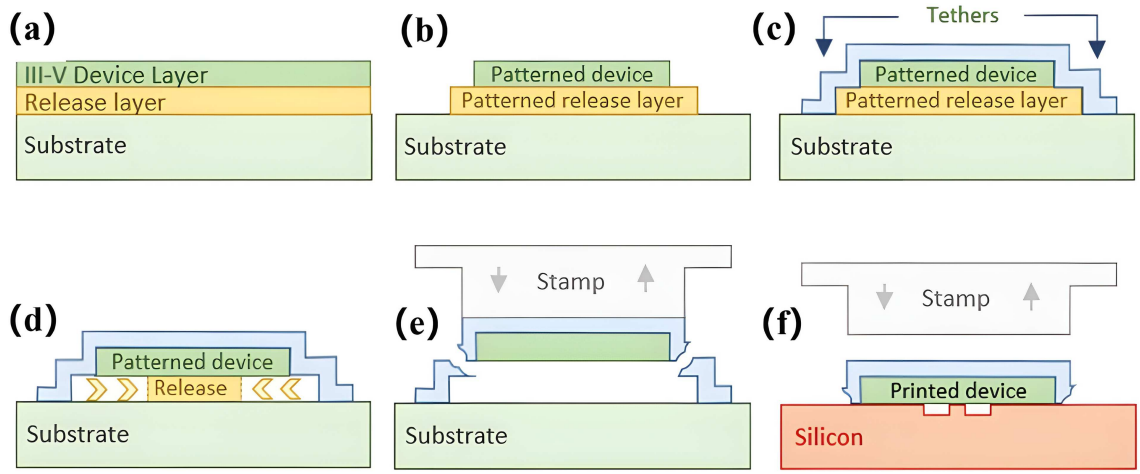

Figure 7 (Color online) Micro-transfer-printing concept illustrating the release, picking, and printing of a single coupon/device. Massively parallel transfer can be achieved using structured stamps [135]. (a) III-V devices are fabricated on donor substrate with release layer; (b) patterning III-V devices and release layer; (c) the definition of tethers on patterned devices; (d) etch release layer; (e) laminating stamp to III-V devices, lifting stamp to break tethers to separate devices from donor substrate; (f) print devices onto silicon target substrate to finish the μTP process.

communication and photonic integration [120, 122].

Beyond lasers, bonding-based methods are commonly used for integrating III-V photodetectors and modulators with waveguide coupling interfaces. These platforms support high-efficiency optoelectronic conversion and enable dense integration of lasers, modulators, and detectors on a single chip. Such systems are poised to meet the growing demands for high-integration, energy-efficient, and cost-effective solutions in next-generation sensing and optical interconnect networks [129–132].

Micro-transfer-printed integration. Micro-transfer-printing (μTP) enables the efficient integration of prefabricated III-V optoelectronic devices onto silicon photonic platforms. Leveraging the viscoelastic properties of a polydimethylsiloxane (PDMS) stamp, this technique offers relaxed alignment tolerance, precise placement, and high material utilization, making it suitable for large-scale parallel manufacturing. Studies have shown that μTP can significantly improve the coupling performance of photonic devices, achieving an average coupling loss as low as 1.26 dB in the C+L bands [133]. Nonetheless, challenges persist in engineering practice, including stamp durability, large-area uniformity, and equipment complexity, with manufacturing costs requiring further optimization [134]. Figure 7 shows a conceptual illustration of the μTP process, comprising six steps: (a) preparation of the III-V source wafer with epitaxial device layers; (b) patterning of the release layer and definition of devices or material coupons; (c) encapsulation of devices with polymer tethers; (d) selective etching of the release layer to free the devices while still held by tethers; (e) breaking of tethers and picking up the devices using a PDMS stamp; (f) transfer and printing of devices onto a silicon photonic wafer with high alignment accuracy [135].

Zhang et al. [135] demonstrated the transfer of III-V DFB lasers (40 μm × 970 μm) onto a silicon photonic platform. Using second-order gratings integrated into silicon waveguides, the devices achieved single-mode lasing at 1550 nm with an SMSR exceeding 40 dB and an output power of 2.2 mW. Figure 8(a) illustrates a heterogeneous

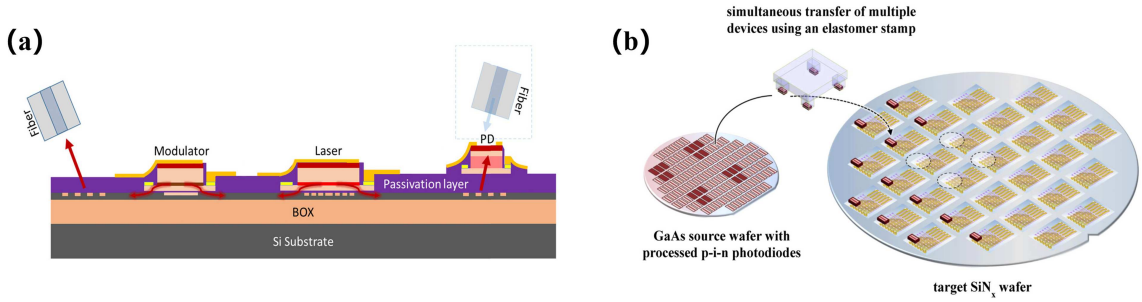

Figure 8 (Color online) (a) Schematic of a photonic circuit based on transfer printing of different III-V epitaxial stacks onto a passive SOI waveguide chip [135]; (b) wafer-scale compatible μTP technology showing the parallel transfer of III-V photodiodes onto SiN_x photonic wafers [140].

photonic integrated circuit on a silicon-on-insulator (SOI) platform. Active components, including modulators, lasers, and photodetectors, are integrated on the same plane, forming a compact and dense layout. Optical interfaces are provided at both ends via fiber couplers, enabling efficient light input and output. This configuration demonstrates the feasibility of integrating multiple III-V and silicon photonic components on a single chip while maintaining planar alignment and interconnectivity. This work validated μTP as an effective route for integrating passive and active devices on the same chip, especially for high-precision laser systems.

Haq et al. [136] transfer-printed III-V optical amplifier structures, fabricated initially on an InP source wafer, onto a SOI platform. The DFB laser was realized using quarter-wave-shifted gratings on SiN waveguides, and tapered couplers were incorporated to enhance mode matching. The device exhibited a threshold current of 80 mA, an output power of 6.9 mW, and an SMSR of 33 dB at 20°C. This method maintains compatibility with standard silicon photonic back-end processes while offering high-throughput and scalable parallel transfer.

Beyond lasers, μTP facilitates integration of broadband light sources and photodetectors. Multiple III-V photonic devices have been transfer-printed in batches onto silicon photonic circuits, forming broadband emitters efficiently coupled to single-mode waveguides [137, 138]. In the short-wavelength regime, silicon p-i-n photodiodes have been printed onto SiN waveguide platforms for sub-850 nm detection, serving applications in biosensing, imaging, and quantum photonics [139]. Similarly, GaAs-based photodiodes have been transferred onto SiN-coupled waveguide structures, achieving up to 47% external quantum efficiency at 860 nm with ultra-low dark currents [140]. As illustrated in Figure 8(b), the micro-transfer-printing process enables prefabricated III-V p-i-n photodiode coupons on a GaAs source wafer to be tethered to the substrate with polymer anchors. The sacrificial release layer beneath the devices is selectively etched, enabling the photodiode coupons to be picked up by a PDMS stamp, thereby severing the tethers during retrieval. These devices are then precisely transferred and printed onto the SiN photonics wafer with high alignment accuracy, achieving dense integration of active III-V detectors with passive waveguides.

In addition to the discussed techniques, conventional hybrid integration methods such as flip-chip bonding and butt coupling continue to remain important in on-chip laser packaging. These methods directly align prefabricated III-V laser chips with silicon or SiN waveguides. Their advantages include prevalidated performance and mature packaging processes. However, they demand submicrometer alignment precision (typically $<\pm 1$ μm), limiting scalability and automation. Coupling efficiency is also sensitive to lateral misalignment [141–143]. Despite these limitations, such methods remain practical for high-power applications and commercial laser modules and may serve as complementary solutions when combined with automated alignment and packaging improvements.

As the foundational element of integrated photonic systems, the performance and integration strategy of on-chip lasers directly impact the overall functional density, power consumption, and scalability. Although bonding offers mature processing and CMOS compatibility, μTP distinguishes itself by its high throughput and platform flexibility. Epitaxial growth remains promising for maximum integration density but is still limited by defect control and lattice mismatch. Flip-chip and butt coupling methods, though simple and high-power-compatible, face precision bottlenecks for dense integration. Understanding these integration strategies and their trade-offs is essential for evaluating laser performance and guiding the design of next-generation on-chip photonic systems. Nevertheless, several engineering challenges persist, including coupling loss, thermal management, packaging complexity, and interface defects. For instance, evanescent coupling is highly sensitive to bonding layer thickness, and improper stress relief during μTP can lead to misalignment and reliability issues. As the primary heat-generating component, the thermal design of the laser also strongly influences long-term system stability.

Table 1 summarizes key performance metrics of DFB laser sources achieved through various integration forms and methods, ranging from off-chip assemblies (discrete and integrated arrays) to on-chip implementations (epitaxy,

Table 1 Performance summary of DFB lasers with different integration methods.

Ref.	Form	Integration method	Laser source type	Center wavelength	Range	Power	SMSR	Linewidth
[92]	Off-chip	Discrete arrays	DFB-arrary	1550 nm	∼3 nm	1.7–4.3 mW	–	1.45–2.55 kHz
[93]	Off-chip	Discrete arrays	DFB-arrary	1550 nm	∼3 nm	1.7–3.3 mW	–	11–63 Hz
[94]	Off-chip	Discrete arrays	DFB-arrary	1550 nm	∼4 nm	–	>40 dB	800 Hz
[95]	Off-chip	Integrated arrays	DFB-arrary	1560 nm	∼3 nm	33 mW	>50 dB	64.3 kHz
[96]	Off-chip	Integrated arrays	DFB-arrary	1653.7 nm	14.4 nm	–	51.4 dB	–
[97]	Off-chip	Integrated arrays	DFB-arrary	1550 nm	∼10 nm	>17 mW	>60 dB	–
[98]	Off-chip	Integrated arrays	DFB-arrary	1653.7 nm	7.2 nm	–	>40 dB	–
[99]	Off-chip	Integrated arrays	DFB-arrary	1550 nm	∼8 nm	15 mW	>48 dB	–
[100]	Off-chip	Integrated arrays	DFB-arrary	1550 nm	∼7 nm	∼10 mW	>36 dB	–
[114]	On-chip	Epitaxy	DFB-arrary	930.5 nm	–	6.4 mW	>20 dB	–
[115]	On-chip	Epitaxy	DFB	629.9 nm	74 nm	–	>20 dB	–
[116]	On-chip	Epitaxy	QD-DFB-arrary	1300 nm	100 nm	0.5 mW	50 dB	–
[103]	On-chip	Epitaxy	DFB-QCL-arrary	4.65 μm	>100 nm	>1.75 W	>20 dB	–
[125]	On-chip	Bonding	DFB	1310 nm	3 nm	2.1 mW	45 dB	–
[126]	On-chip	Bonding	DFB	1550 nm	–	14 mW	50 dB	1 MHz
[127]	On-chip	Bonding	DFB	1300 nm	30 nm	>15 mW	50 dB	–
[128]	On-chip	Bonding	DFB	1310 nm	0.42 nm	5 mW	–	–
[135]	On-chip	μTP	DFB	1550 nm	–	2.2 mW	40 dB	–
[136]	On-chip	μTP	DFB	1558 nm	<2 nm	9.1 mW	30 dB	–

bonding, and micro-transfer-printing). The table enumerates center wavelength, tuning range, output power, SMSR, and linewidth, highlighting the inherent trade-offs across different platforms. Off-chip arrays achieve exceptionally narrow free-running linewidths (down to tens of hertz) and high SMSR, but rely on external coupling and packaging. On-chip approaches increasingly bridge this performance gap: epitaxial arrays provide broadband coverage (up to ∼100 nm) with dense integration, bonding enables CMOS-compatible devices with sub-MHz linewidths, and μTP offers high-throughput, material-agnostic placement with competitive SMSR. Across the reported data, linewidths span from ∼10 Hz to ∼1 MHz, SMSR typically exceeds 40–50 dB, and wavelength agility ranges from sub-nanometer to >100 nm, directly corresponding to distinct sensing applications.

From a sensing perspective, three laser-source parameters dominate system-level performance: narrow linewidth, high SMSR, and wide tunability. These laser characteristics directly translate into system-level benefits across diverse applications. In spectroscopic sensing, narrow linewidths on the order of tens of kHz to sub-MHz and high spectral purity enhance resolution and detection sensitivity by enabling precise frequency locking to molecular absorption features; this is critical in trace-gas analysis and selective PAS measurements [144–146]. High SMSR, typically exceeding 40–50 dB, ensures stable single-longitudinal-mode operation, suppressing multimode interference and stabilizing signal readout. Additionally, active techniques such as injection locking or feedback control can further compress linewidth and improve frequency stability [147–150]. In coherent LiDAR, laser coherence and frequency stability determine ranging precision and noise resilience; narrow-linewidth sources (down to kHz-level) reduce phase noise and improve interferometric signal-to-noise ratio, with chip-scale comb and feedback techniques demonstrating linewidth compression from MHz to kHz under eye-safe power constraints [151–155]. For quantum communication, single-mode stability (high SMSR >40 dB) and narrow linewidths (∼100 kHz) maintain photon coherence over long distances; electrically controlled quantum-dot emitters and cavity-enhanced coupling improve brightness, indistinguishability, and temperature robustness, whereas electrical or strain tuning aligns emission to telecom bands for multiwavelength QKD [156–162]. Taken together, these considerations suggest that for high-resolution spectroscopy, coherent ranging, and quantum communication, DFB or quantum-dot lasers with linewidths below ∼100 kHz, SMSR above 40 dB, and tunability spanning tens of nanometers can effectively satisfy system-level performance requirements.

Overall, Table 1 quantifies laser performance and highlights critical design considerations for next-generation on-chip photonic sensing. Narrow linewidths (Hz–kHz) with >40 dB SMSR favor high-resolution spectroscopy and coherent ranging, whereas wavelength tunability spanning tens to hundreds of nanometers supports multi-species gas detection and channelized sensing. The choice among epitaxy, bonding, and μTP determines how these metrics scale with footprint, yield, and platform flexibility. These insights motivate a clear developmental trajectory: advancing from stand-alone devices toward co-designed, fully integrated on-chip subsystems, in which lasers are tightly coupled with modulators, detectors, filters, and driving electronics. For sensing applications, key system-level factors—including output stability, tuning linearity and range, and passive alignment precision—will

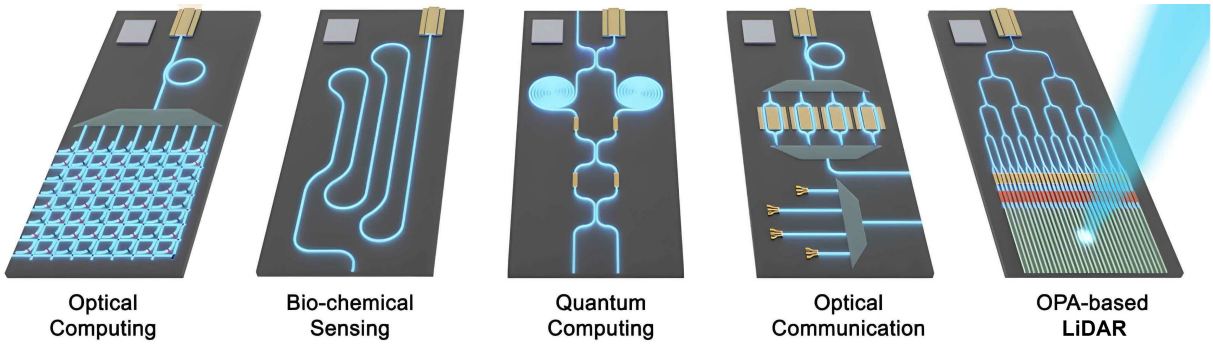

Figure 9 (Color online) Schematic of III-V-on-chip system based on different application areas [163].

ultimately dictate performance. Consequently, moving from device-level integration to holistic system-level co-design represents a pivotal pathway toward high-performance, densely integrated, and scalable photonic sensing chips. These considerations naturally lead to the exploration of fully integrated III-V-on-chip systems for multi-functional photonic sensing.

4 Integrated III-V-on-chip systems for multi-functional photonic sensing

Amid the continued advancement of integrated photonics, on-chip sensing systems are transitioning from single-function component integration toward system-level, multimodule cooperation. III-V semiconductor lasers, with their high gain, wide wavelength tunability, and superior thermal stability, are the core of on-chip light sources. Their integration with modulators, passive waveguides, photodetectors, and filters has enabled stable, tunable, and high-power laser output, laying the foundation for compact, energy-efficient, and scalable multi-functional photonic systems. These integrated platforms have demonstrated compelling advantages in applications such as spectroscopic sensing, environmental monitoring, quantum communication, optical computing, and FMCW LiDAR. The structure of the on-chip laser source integration system across application domains is shown in Figure 9 [163].

4.1 Spectroscopic sensing systems

In the field of on-chip spectroscopic sensing, the integration of III-V light sources with silicon photonic circuits offers a promising route toward compact, low-cost, and high-sensitivity spectrometer systems. Figure 10(a) displays a silicon photonic integrated circuit operating in the 2–4 μm mid-infrared range, which incorporates DFB lasers, photodetectors, and waveguide-based arrayed waveguide gratings (AWGs) on a single SOI chip [164]. The 2.3 μm DFB lasers utilize InP epitaxial layers and exhibit single-mode output power of 3 mW. By adjusting the grating period and waveguide width, the laser array spans 2.28–2.43 μm, and a continuous current-tuning range exceeding 10 nm is additionally achieved by fabricating four DFB lasers with different waveguide widths. The AWG spectrometer integrates an adiabatically coupled InP-based type-II quantum well photodetector array, with each AWG channel coupled to a photodetector spaced 60 μm apart. This configuration enables wavelength demultiplexing and facilitates direct interfacing with electronic components, enhancing the scalability of the integrated spectroscopic system. The integrated photodetectors feature a responsivity of 1.6 A/W at 2.35 μm with dark currents below 10 nA. The AWG spectrometer offers low insertion loss (2–3 dB) and excellent channel isolation (<-30 dB), enabling precise multiband spectroscopic measurements.

To enable high-sensitivity, low-power, and cost-effective real-time monitoring of greenhouse gases such as methane, a tunable diode laser absorption spectroscopy (TDLAS)-based gas sensor chip was developed. The system integrates a tunable external-cavity emitter, a 30 cm-long evanescent-field silicon waveguide, an on-chip hermetically sealed reference gas cell, and a monolithically integrated detector, forming a compact and fully functional sensing loop [165]. Wavelength self-calibration is achieved through the integrated reference cavity, ensuring robust operation with minimal power consumption while maintaining high spectral resolution and stability. The coiled silicon waveguides interrogate ambient methane via the evanescent field of the guided mode, and the on-chip reference cell provides a stable absorption signal for accurate wavelength locking and baseline normalization.

Meyer et al. [166] developed a mid-infrared sensing platform based on GaSb-based ICLs, achieving platform-level integration through bonding, and fully monolithically integrating lasers, detectors, and passive waveguides within a III-V material stack. As shown in Figure 10(b), the architecture supports evanescent coupling-based detection and embeds waveguides and detectors within the laser cavity, forming a compact, low-loss sensing loop. Highly

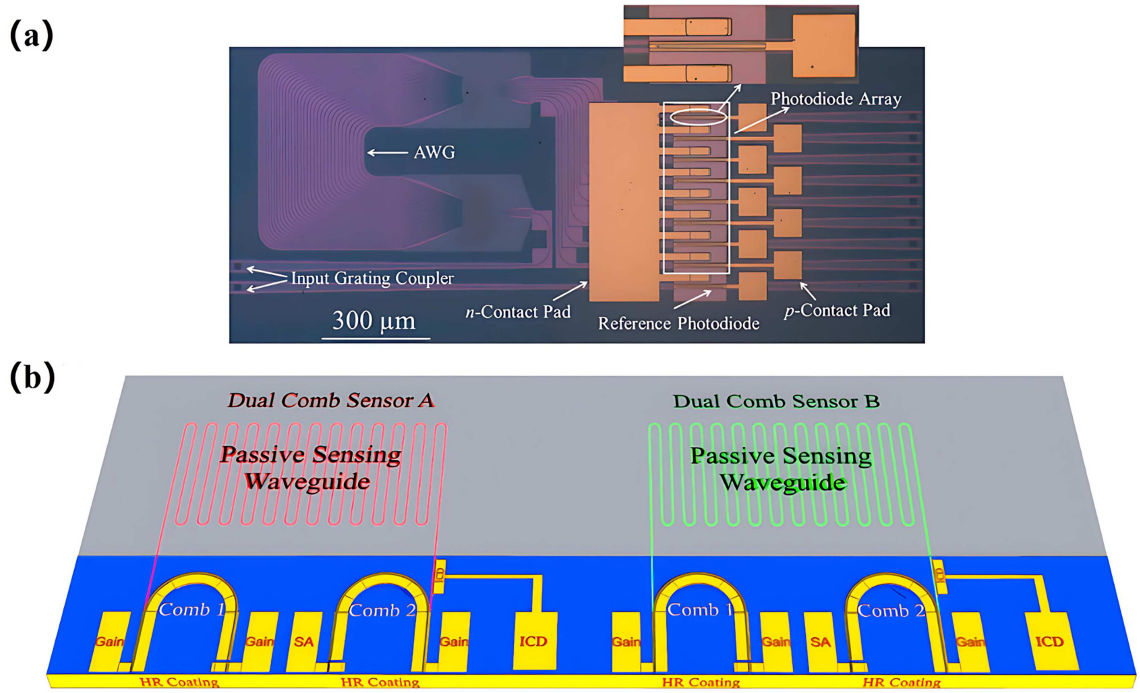

Figure 10 (Color online) (a) Microscope image of a 2.3 μm AWG spectrometer monolithically integrated with an InP-based type-II quantum well photodetector array on a silicon photonic platform [164]; (b) schematic of a photonic integrated circuit (PIC) combining multiple ICLs, detectors, and dual-comb spectrometers, with sensing waveguides positioned to directly interact with ambient gases [166].

reflective facet designs enable cavity lengths below 0.3 mm and driving powers under 10 mW. Although GaSb-based processing lags InP and silicon photonics in maturity, its compatibility with existing MIR device processes offers scalability and strong application potential.

4.2 LiDAR and quantum communication systems

In the area of coherent frequency-modulated continuous-wave (FMCW) LiDAR, Poulton et al. [167] fabricated a fully integrated transmitter-receiver chip using standard silicon photonic processes. This chip integrates Mach-Zehnder modulators, OPA emitters and receivers, germanium photodetectors, and thermal phase shifters. A DFB laser source is coupled externally via fiber for frequency-swept operation. The system achieves centimeter-level distance resolution over a 20 mm range and supports a maximum ranging capability of up to 2 m, with a compact footprint of 6 mm × 0.5 mm, indicating high manufacturability and integration potential.

Yue et al. [168] proposed a two-dimensional OPA LiDAR system combining a tunable MQW laser array with beamforming components, all fabricated on an SOI platform. As shown in Figure 11(a), this work demonstrates a heterogeneous integration approach on a silicon photonic platform, combining two-dimensional (2D) OPA with tunable MQW laser arrays. The 2D OPA chip consists of four main components: tunable MQW laser arrays, an electro-optic (EO) switch array for signal selection, an EO phase-shifter array, and a Bragg waveguide grating antenna array. Four groups of InP MQW lasers bonded onto the silicon chip emit in the 1480–1600 nm wavelength range, with inter-group spacing of approximately 30 nm and inter-laser spacing of 3.75 nm. The chip footprint is only 8 mm × 3 mm, and the switching time can reach 2.5 ps, offering a promising solution for ultra-compact, high-speed, and high-precision LiDAR systems.

For quantum communication, particularly continuous-variable quantum key distribution (CV-QKD), an integrated silicon photonic platform has been demonstrated, incorporating amplitude and phase modulators, polarization multiplexers, local oscillator injection, demultiplexers, and balanced photodetectors [169]. As shown in Figure 11(b), the system implements Gaussian modulation and homodyne detection within a single chip, with the amplitude and phase modulators based on Mach-Zehnder interferometers achieving a 90% switching time of 2.5 ns, corresponding to a 200 MHz modulation frequency. Limited by the detector bandwidth, the system operates between 1–10 MHz, within the optimal range of the modulators, whereas cross-modulation measurements confirm negligible interaction between the amplitude and phase modulators. The transmitter chip is packaged on a printed circuit board (PCB), significantly reducing system complexity and power consumption. Although the laser

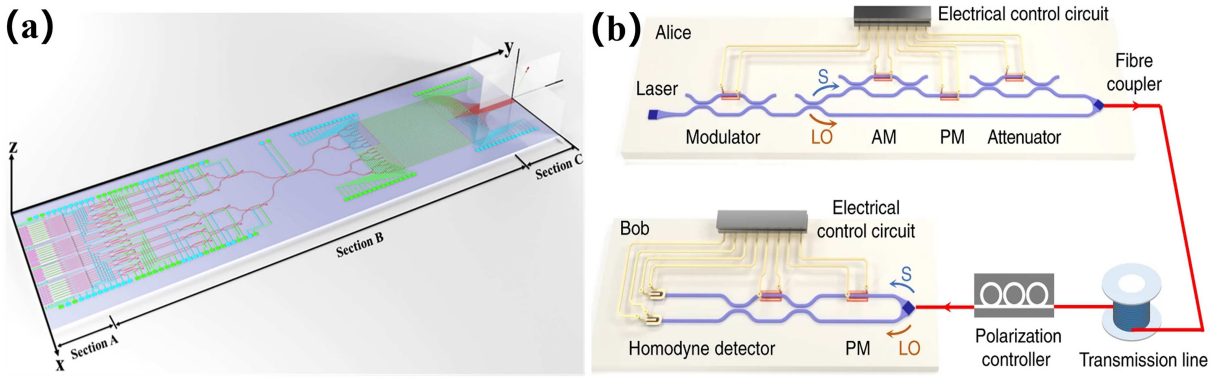

Figure 11 (Color online) (a) Schematic of a 2D optical phased array (OPA) LiDAR system integrating a tunable MQW laser array, electro-optic switches, phase modulators, and grating antenna arrays on an SOI platform [168]; (b) diagram of an integrated CV-QKD transceiver chip, where Alice and Bob each comprise amplitude/phase modulators, attenuators, and demultiplexers, enabling polarization multiplexing and homodyne detection [169].

remains off-chip in this design, further integration of III-V lasers is expected to enable fully monolithic, cost-effective CV-QKD systems.

4.3 Optical communication systems

In the domain of optical communication, tunable semiconductor lasers play a crucial role in DWDM and high-performance interconnects. Wan et al. [170] achieved direct growth of single-wavelength quantum dot lasers on standard (001) silicon substrates using a one-step epitaxial process, integrated with cascaded half-wave-coupled ring resonators for on-chip tuning. As shown in Figure 12(a), the laser employs two all-active ring resonators coupled to a common Fabry-Pérot cavity via half-wave couplers, enabling robust wavelength selectivity without the need for gratings or thermoelectric cooler (TEC) tuning. This architecture enables more than 16 nm of continuous tuning, with demonstrated 11- and 37-channel switching. The device delivers output powers above 2.7 mW per channel and achieves SMSR up to 45 dB.

Ren et al. [171] reported a silicon photonic tunable laser using a flip-chip bonded gain chip coupled to a pair of ring resonators acting as a reflector in the external cavity. As shown in Figure 12(b), the complementary thermo-optic and free-carrier tuning schemes enable a wide tuning range of 41.6 nm with fine resolution down to 2 pm. The device achieves 2 mW output power, SMSR above 40 dB, and sub-nanosecond response times, supported by an external-cavity efficiency of 22%. This architecture highlights the efficacy of coupled-ring resonators in providing flexible and precise wavelength control for integrated silicon photonic systems.

Pan et al. [172] developed a narrow-linewidth tunable laser on Si_3N_4 using micro-transfer-printed III-V gain chips integrated onto a low-loss LPCVD Si_3N_4 platform (Figure 12(c)). The device employs cascaded microring resonator (MRR) mirrors with Vernier tuning, assisted by micro-heaters and vertical couplers, enabling a 54 nm tuning range across the C+L bands. It achieves an intrinsic linewidth below 25 kHz, a side-mode suppression ratio (SMSR) above 40 dB, and an output power up to 6.3 mW. This transfer-based heterogeneous integration demonstrates high performance and reproducibility and shows scalability toward large-volume photonic integration.

III-V semiconductor lasers have evolved from single-function sources to core elements of fully integrated on-chip photonic sensing systems. Their high compatibility with silicon and silicon nitride platforms supports compact packaging, power efficiency, and cost-effective manufacturing. These lasers enable practical systems in mid-infrared spectroscopy, quantum communication, LiDAR, and DWDM. Future developments in material growth, wafer-scale transfer, and AI-enabled control may push the limits of bandwidth, energy efficiency, and environmental resilience, driving III-V-on-chip sensing systems toward widespread deployment in healthcare, environmental monitoring, IoT, and quantum photonics [173–179].

5 Outlook and conclusion

This review comprehensively summarizes the recent progress of DFB lasers based on III-V materials, covering the material platforms, device structures, and integration technologies across all key spectral regimes. In the visible regime, GaN and its related alloys are a pivotal III-V platform, enabling high-performance laser operation for applications in visible-light communication, underwater optical links, and sensing. In the NIR regime, well-established

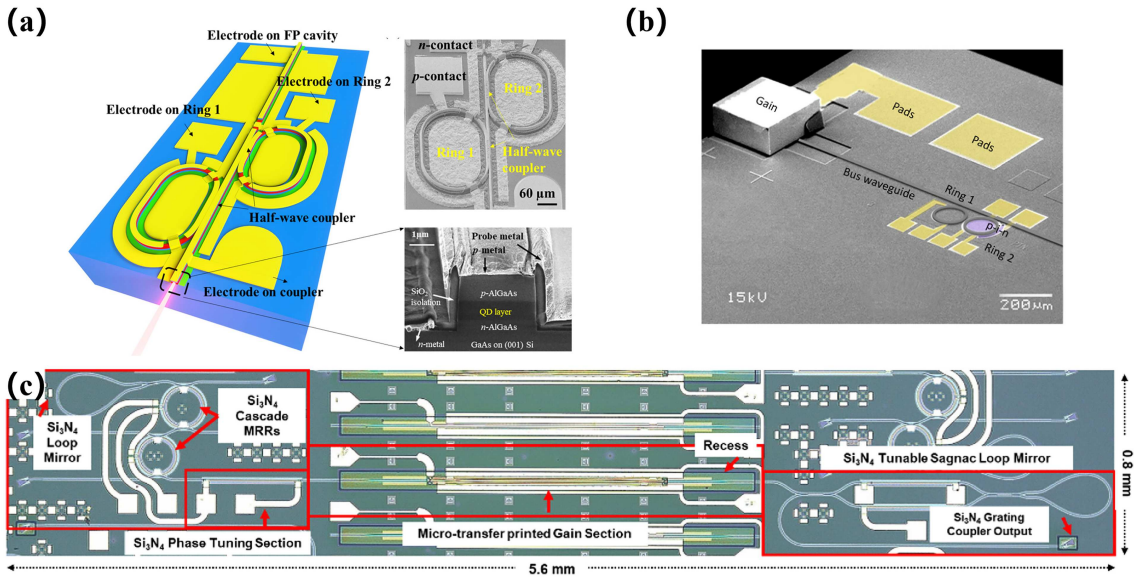

Figure 12 (Color online) (a) Schematic, top-view SEM, and cross-sectional SEM images of a tunable quantum dot laser monolithically grown and integrated with coupled ring resonators on silicon [170]; (b) SEM image of a silicon photonic tunable laser using a pair of coupled ring resonators as feedback elements [171]; (c) microscope image of a III-V-on-Si_3N_4 tunable narrow-linewidth laser fabricated via micro-transfer-printing for low-loss C+L band applications [172].

QW platforms based on GaAs and InP offer excellent optoelectronic performance and fabrication maturity, finding widespread use in high-speed communication and biomedical sensing. In the MIR band, the adoption of antimonide-based compounds significantly broadens the accessible emission range and enables multi-species gas sensing and infrared spectroscopy. In the FIR regime, QCLs reach longer wavelengths, offering powerful solutions for long-wave infrared applications. Driven by continuous innovations in materials, cavity designs, and integration strategies, III-V DFB lasers are in use across diverse fields such as molecular detection, environmental analysis, free-space optical links, and quantum information processing.

At the material level, the incorporation of QDs as gain media introduces strong carrier confinement, spectrally selective gain, and superior temperature robustness. These attributes are particularly valuable for mid-infrared DFB lasers, enhancing performance in trace gas detection applications and enabling broadband, high-sensitivity spectroscopic systems.

At the structural level, DFB lasers are evolving from discrete single-mode sources to integrated multichannel arrays. Multi-wavelength DFB arrays—implemented either discretely or monolithically—enable synchronized detection of multiple gas species via spectroscopic techniques such as WMS and TDLAS. Furthermore, the realization of on-chip laser sources through approaches such as direct epitaxy, wafer-level bonding, and micro-transfer-printing enables significant reductions in footprint, power consumption, and system complexity. These developments underpin the creation of highly scalable integrated photonic platforms.

Building on these advances, on-chip sensing systems based on III-V DFB sources are a core research frontier. By co-integrating DFB laser arrays with modulators, waveguides, filters, and detectors, fully functional photonic systems capable of spectral scanning, environmental monitoring, gas identification, and quantum communication have been demonstrated. Notable examples include high-resolution mid-infrared AWG spectrometers, ultralow-power TDLAS chips, compact OPA-LiDAR transceivers, and CV-QKD quantum photonic modules. These systems underscore the feasibility of III-V-on-chip photonic architectures in intelligent sensing applications across diverse scenarios.

Looking ahead, the development of DFB laser sources stands to gain through ongoing advances in epitaxial growth control, ultralow-loss waveguide coupling, higher-order feedback engineering, and AI-assisted device optimization. In synergy with multimodal sensing frameworks, machine learning algorithms, and photonic-electronic co-design strategies, III-V-based on-chip sensing platforms are poised to become a foundational element in next-generation photonic systems—enabling breakthroughs in smart manufacturing, environmental monitoring, medical diagnostics, and quantum information technologies. These systems promise enhanced bandwidth, lower energy consumption, and improved environmental adaptability, marking a key step toward fully integrated, high-performance photonic systems.

Acknowledgements This work was supported by National Key R&D Program of China (Grant No. 2022YFB2804501), National Natural Science Foundation of China (Grant Nos. 62090052, 62121005, 62227819, 62274164, 62275245, 62090054), Science and Technology Development Project of Jilin Province (Grant Nos. 20210301016GX, 20240302004GX, 20250601088RC, 20230508097RC, 20220201072GX), Greenhouse Gas Monitoring Instrument Project of Ministry of Industry and Information Technology (Grant No. ZTZB-23-990-003), and Dawn Talent Training Program of CIOMP.

References

1 Chang J, Gao J, Esmaeil Zadeh I, et al. Nanowire-based integrated photonics for quantum information and quantum sensing. Nanophotonics, 2023, 12: 339–358
2 Atabaki A H, Moazeni S, Pavanello F, et al. Integrating photonics with silicon nanoelectronics for the next generation of systems on a chip. Nature, 2018, 556: 349–354
3 Xu L, Dai Z, Duan G, et al. Micro/nano gas sensors: a new strategy towards in-situ wafer-level fabrication of high-performance gas sensing chips. Sci Rep, 2015, 5: 10507
4 Momenbeitollahi N, Cloet T, Li H. Pushing the detection limits: strategies towards highly sensitive optical-based protein detection. Anal Bioanal Chem, 2021, 413: 5995–6011
5 Kitaw S L, Birhan Y S, Tsai H C. Plasmonic surface-enhanced Raman scattering nano-substrates for detection of anionic environmental contaminants: current progress and future perspectives. Environ Res, 2023, 221: 115247
6 Meyer S A, Le Ru E C, Etchegoin P G. Combining surface plasmon resonance (SPR) spectroscopy with surface-enhanced raman scattering (SERS). Anal Chem, 2011, 83: 2337–2344
7 Culleton L P, di Meane E A, Ward M K M, et al. Characterization of Fourier transform infrared, cavity ring-down spectroscopy, and optical feedback cavity-enhanced absorption spectroscopy instruments for the analysis of ammonia in biogas and biomethane. Anal Chem, 2022, 94: 15207–15214
8 Selvaraj R, Vasa N J, Shiva Nagendra S M. Off-resonance photoacoustic spectroscopy technique for multi-gas sensing in biogas plants. Anal Chem, 2019, 91: 14239–14246
9 Chen J P, Zhang C, Liu Y, et al. Quantum key distribution over 658 km fiber with distributed vibration sensing. Phys Rev Lett, 2022, 128: 180502
10 Li Y, Wang Z, Du H, et al. Integrated communication and sensing system based on Si-SiN dual-layer optical phased array. Opt Express, 2024, 32: 33222–33231
11 Yang D, Yan F, Guo Y, et al. Suppression of intensity noise and phase noise for thulium-holmium co-doped fiber laser by self-injection locking. Opt Express, 2024, 32: 33521–33530
12 Wei W Q, He A, Yang B, et al. Monolithic integration of embedded III-V lasers on SOI. Light Sci Appl, 2023, 12: 84
13 Hu Y, Liang D, Mukherjee K, et al. III/V-on-Si MQW lasers by using a novel photonic integration method of regrowth on a bonding template. Light Sci Appl, 2019, 8: 93
14 Karami Keshmarzi E, Tait R N, Berini P. Single-mode surface plasmon distributed feedback lasers. Nanoscale, 2018, 10: 5914–5922
15 Yao D Y, Zhang J C, Cathabard O, et al. 10-W pulsed operation of substrate emitting photonic-crystal quantum cascade laser with very small divergence. Nanoscale Res Lett, 2015, 10: 177
16 Feng C, Giglio M, Li B, et al. Detection of hydrogen sulfide in sewer using an erbium-doped fiber amplified diode laser and a gold-plated photoacoustic cell. Molecules, 2022, 27: 6505
17 Wang D B, Zhang J C, Cheng F M, et al. Stable single-mode operation of distributed feedback quantum cascade laser by optimized reflectivity facet coatings. Nanoscale Res Lett, 2018, 13: 37
18 Lv Z, Liu X, Wu S, et al. Massive GaN micro-LED array based underwater wireless optical communication. Opt Express, 2025, 33: 19527–19534
19 Li G, Hu F, Zou P, et al. Advanced modulation format of probabilistic shaping bit loading for 450-nm GaN laser diode based visible light communication. Sensors, 2020, 20: 6143
20 Geum D M, Lim J, Jang J, et al. Highly-efficient (>70%) and wide-spectral (400–1700 nm) sub-micron-thick InGaAs photodiodes for future high-resolution image sensors. Light Sci Appl, 2024, 13: 311
21 Zeller W, Naehle L, Fuchs P, et al. DFB lasers between 760 nm and 16 μm for sensing applications. Sensors, 2010, 10: 2492–2510
22 Yan Z, Han Y, Lin L, et al. A monolithic InP/SOI platform for integrated photonics. Light Sci Appl, 2021, 10: 1–10
23 Hümmer M, Rößner K, Lehnhardt T, et al. Long wavelength GaInAsSb-AlGaAsSb distributed-feedback lasers emitting at 2.84 μm. Electron Lett, 2006, 42: 1
24 Park A H, Seo T H, Chandramohan S, et al. Efficient stress-relaxation in InGaN/GaN light-emitting diodes using carbon nanotubes. Nanoscale, 2015, 7: 15099–15105
25 Zhou S, Liu X, Yan H, et al. The effect of nanometre-scale V-pits on electronic and optical properties and efficiency droop of GaN-based green light-emitting diodes. Sci Rep, 2018, 8: 11053
26 Yu Y, Wang T, Chen X, et al. Demonstration of epitaxial growth of strain-relaxed GaN films on graphene/SiC substrates for long wavelength light-emitting diodes. Light Sci Appl, 2021, 10: 117
27 Jentsch S A, Zscherp M F, Lider V, et al. Metal-modulated growth of cubic, red-emitting InGaN layers and self-assembled InGaN/GaN quantum wells by molecular beam epitaxy. ACS Appl Electron Mater, 2025, 7: 1891–1898
28 Ikeda K, Kawai K, Kametani J, et al. Spatial and time-resolved properties of emission enhancement in polar/semi-polar InGaN/GaN by surface plasmon resonance. Nanophotonics, 2024, 13: 1435–1447
29 Sun Y, Zhou K, Feng M, et al. Room-temperature continuous-wave electrically pumped InGaN/GaN quantum well blue laser diode directly grown on Si. Light Sci Appl, 2018, 7: 13
30 Chen L, Xie S, Lan J, et al. High-speed and high-responsivity blue light photodetector with an InGaN NR/PEDOT: PSS heterojunction decorated with Ag NWs. ACS Appl Mater Interfaces, 2024, 16: 29477–29487
31 Lee C, Zhang C, Cantore M, et al. 4 Gbps direct modulation of 450 nm GaN laser for high-speed visible light communication. Opt Express, 2015, 23: 16232–16237
32 Holguin-Lerma J A, Kong M, Alkhazragi O, et al. 480-nm distributed-feedback InGaN laser diode for 10.5-Gbit/s visible-light communication. Opt Lett, 2020, 45: 742–745
33 Liu X, Yi S, Zhou X, et al. 345 m underwater optical wireless communication with 270 Gbps data rate based on a green laser diode with NRZ-OOK modulation. Opt Express, 2017, 25: 27937–27947

34 Wang J, Tian C, Yang X, et al. Underwater wireless optical communication system using a 16-QAM modulated 450-nm laser diode based on an FPGA. Appl Opt, 2019, 58: 4553–4559
35 Qin L J, Zhu J J, Zhang B W, et al. Al_2O_3/AlN/GaN MOS-HEMTs on 6-inch silicon substrate with high transconductance and state-of-the-art $f_{\max} \times L_G$. Sci China Inf Sci, 2025, 68: 139403
36 Luan J, Han Y, Yang S, et al. Experiment demonstration of high speed 1.3 μm grating assisted surface-emitting DFB lasers. Opt Express, 2022, 30: 25111–25120
37 Han Y, Tian Q, Yang S, et al. Direct modulation bandwidth enhancement of uncooled DFB laser operating over a wide temperature range based on groove-in-trench waveguide structure. Opt Express, 2022, 30: 15757–15765
38 Yao M, Sheng C, Ge M, et al. Facile five-step heteroepitaxial growth of GaAs nanowires on silicon substrates and the twin formation mechanism. ACS Nano, 2016, 10: 2424–2435
39 Li B, Yan X, Zhang X, et al. Self-catalyzed growth of InAs nanowires on InP substrate. Nanoscale Res Lett, 2017, 12: 34
40 Haas J, Stach R, Kolm C, et al. Gallium arsenide waveguides as a platform for direct mid-infrared vibrational spectroscopy. Anal Bioanal Chem, 2020, 412: 3447–3456
41 Granger G, Bailly M, Delahaye H, et al. GaAs-chip-based mid-infrared supercontinuum generation. Light Sci Appl, 2023, 12: 252
42 Tang L, Chun I S, Wang Z, et al. DNA detection using plasmonic enhanced near-infrared photoluminescence of gallium arsenide. Anal Chem, 2013, 85: 9522–9527
43 Ivascu I R, Matei C E, Patachia M, et al. CO_2 laser photoacoustic measurements of ethanol absorption coefficients within infrared region of 9.2–10.8 μm. SpectroChim Acta Part A-Mol Biomol Spectr, 2016, 163: 115–119
44 Yu H, Yang C, Chen Y, et al. Mid-infrared high-power InGaAsSb/AlGaInAsSb multiple-quantum-well laser diodes around 2.9 μm. Nanomaterials, 2025, 15: 139
45 Cheng'ao Y, Shengwen X, Shushan H, et al. Research progress of antimonide infrared single mode semiconductor laser. Infrared and Laser Eng, 2018, 47: 503002
46 Han S X, Yan J Y, Cao C F, et al. Single-mode GaSb-based laterally coupled distributed-feedback laser for CO_2 gas detection. Chinese Phys B, 2023, 32: 104205
47 Huang Y H, Yang Z X, Cheng S L, et al. Effect of hole shift on threshold characteristics of GaSb-based double-hole photonic-crystal surface-emitting lasers. Micromachines, 2021, 12: 468
48 Pan C H, Lin C H, Chang T Y, et al. GaSb-based mid infrared photonic crystal surface emitting lasers. Opt Express, 2015, 23: 11741–11747
49 Li Z L, Lin S C, Lin G, et al. Effect of etching depth on threshold characteristics of GaSb-based middle infrared photonic-crystal surface-emitting lasers. Micromachines, 2019, 10: 188
50 Milde T, Assmann C, Jimenez A, et al. Single mode GaSb diode lasers for sensor applications in a long wavelength regime. Appl Opt, 2017, 56: H45
51 Cui X, Yu R, Chen W, et al. Development of a quantum cascade laser-based sensor for environmental hono monitoring in the mid-infrared at 8 μm. J Lightwave Technol, 2018, 37: 2784–2791
52 Tittel F K, Allred J J, Cao Y, et al. Quantum cascade laser-based sensor system for nitric oxide detection. In: Proceedings of the SPIE, 2015. 164–170
53 Rowlette J, Takeuchi E, Day T. QCL applications in scientific research, commercial, and defense and security markets. In: Mid-Infrared and Terahertz Quantum Cascade Lasers. Cambridge: Cambridge University Press, 2023. 373
54 Consolino L, Cappelli F, de Cumis M S, et al. QCL-based frequency metrology from the mid-infrared to the THz range: a review. Nanophotonics, 2019, 8: 181–204
55 Wang F, Slivken S, Razeghi M. High-brightness LWIR quantum cascade lasers. Opt Lett, 2021, 46: 5193–5196
56 Scalari G, Faist J. 30 years of the quantum cascade laser. Commun Phys, 2024, 7: 394
57 Pinto D, Díaz Thomas D A, Loghmari Z, et al. Long wavelength distributed feedback tapered quantum cascade lasers. Opt Express, 2024, 32: 26925–26937
58 Zhang J, Peng H, Wang J, et al. Dense spectral beam combining of quantum cascade lasers by multiplexing a pair of blazed gratings. Opt Express, 2022, 30: 966–971
59 Abramov P I, Budarin A S, Kuznetsov E V, et al. Quantum-cascade lasers in atmospheric optical communication lines: challenges and prospects (review). J Appl Spectrosc, 2020, 87: 579–600
60 Tang P, Chi X, Chen B, et al. Predictions of resonant mode characteristics for terahertz quantum cascade lasers with distributed feedback utilizing machine learning. Opt Express, 2021, 29: 15309–15326
61 Hashimoto J, Yoshinaga H, Mori H, et al. Low power-consumption mid-infrared distributed feedback quantum cascade laser for gas-sensing application. Electron Lett, 2017, 53: 549–551
62 Cheng F M, Zhang J C, Wang D B, et al. Demonstration of high-power and stable single-mode in a quantum cascade laser using buried sampled grating. Nanoscale Res Lett, 2019, 14: 123
63 Marschick G, Pelini J, Gabbrielli T, et al. Mid-infrared ring interband cascade laser: operation at the standard quantum limit. ACS Photonics, 2024, 11: 395–403
64 Yang H, Yang R Q, Gong J, et al. Mid-infrared widely tunable single-mode interband cascade lasers based on V-coupled cavities. Opt Lett, 2020, 45: 2700–2703
65 Frank F, Baumgartner B, Verstuyft M, et al. Integrated optics waveguides and mesoporous oxides for the monitoring of volatile organic compound traces in the mid-infrared. Appl Spectrosc, 2025, 79: 842–851
66 Liao C S, Blanchard R, Pfluegl C, et al. Portable broadband photoacoustic spectroscopy for trace gas detection by quantum cascade laser arrays. Opt Lett, 2020, 45: 3248–3251
67 Gadedjisso-Tossou K S, Stoychev L I, Mohou M A, et al. Cavity ring-down spectroscopy for molecular trace gas detection using a pulsed DFB QCL emitting at 6.8 μm. Photonics, 2020, 7: 74
68 Murata M, Yoshinaga H, Mori H, et al. High sensitive gas sensing with low power consumption quantum cascade lasers. Sei Techn Rev, 2016, 83: 40–44
69 Mei Y, Weng G E, Zhang B P, et al. Quantum dot vertical-cavity surface-emitting lasers covering the 'green gap'. Light Sci Appl, 2017, 6: e16199
70 La Rosa M, Payne E H, Credi A. Semiconductor quantum dots as components of photoactive supramolecular architectures. ChemistryOpen, 2020, 9: 200–213

71 Mancini L, Moyon F, Hernàndez-Maldonado D, et al. Carrier localization in GaN/AlN quantum dots as revealed by three-dimensional multimicroscopy. Nano Lett, 2017, 17: 4261–4269
72 Hu Y, Xin K Y, Qiu S Q, et al. Recent progress and challenges of infrared quantum dots. Sci China Inf Sci, 2025, 68: 181401
73 Zhukov A E, Kryzhanovskaya N V, Moiseev E I, et al. Quantum-dot microlasers based on whispering gallery mode resonators. Light Sci Appl, 2021, 10: 80
74 Liu G, Poole P J, Lu Z, et al. InAs/InP quantum dot mode-locked laser with an aggregate 12.544 Tbit/s transmission capacity. Opt Express, 2022, 30: 3205–3214
75 Yuan Q, Liang B, Luo S, et al. Type-II GaSb quantum dots grown on InAlAs/InP (001) by droplet epitaxy. Nanotechnology, 2020, 31: 315701
76 Jiang C, Ning J, Li X, et al. Development of a 1550-nm InAs/GaAs quantum dot saturable absorber mirror with a short-period superlattice capping structure towards femtosecond fiber laser applications. Nanoscale Res Lett, 2019, 14: 362
77 Uvin S, Kumari S, De Groote A, et al. 13 μm InAs/GaAs quantum dot DFB laser integrated on a Si waveguide circuit by means of adhesive die-to-wafer bonding. Opt Express, 2018, 26: 18302–18309
78 Abdollahinia A, Banyoudeh S, Rippien A, et al. Temperature stability of static and dynamic properties of 155 μm quantum dot lasers. Opt Express, 2018, 26: 6056–6066
79 Yuan H H, Gao F, Yang T. Ultra-broadband tunable single- and double-mode InAs/InP quantum dot external-cavity laser emitting around 1.65 μm. Opt Lett, 2018, 43: 3025–3028
80 Mao M H, Chien H C, Hong J Z, et al. Room-temperature low-threshold current-injection InGaAs quantum-dot microdisk lasers with single-mode emission. Opt Express, 2011, 19: 14145–14151
81 Xu B, Wang G, Du Y, et al. Monolithic integration of O-band InAs quantum dot lasers with engineered GaAs virtual substrate based on silicon. Nanomaterials, 2022, 12: 2704
82 Shuhui Z, Lu W, Zhenwu S, et al. The structural and optical properties of GaSb/InGaAs type-II quantum dots grown on InP (100) substrate. Nanoscale Res Lett, 2012, 7: 87
83 Mexis M, Sergent S, Guillet T, et al. High quality factor nitride-based optical cavities: microdisks with embedded GaN/Al(Ga)N quantum dots. Opt Lett, 2011, 36: 2203–2205
84 Lv Z, Zhang S, Jiang H. Superhigh gain InGaN/GaN visible-light photodetector using polarization heterointerface barrier and single-carrier superlattices. Opt Express, 2024, 32: 22045–22051
85 Barettin D, Auf der Maur M, di Carlo A, et al. Carrier transport and emission efficiency in InGaN quantum-dot based light-emitting diodes. Nanotechnology, 2017, 28: 275201
86 Kwoen J, Jang B, Watanabe K, et al. High-temperature continuous-wave operation of directly grown InAs/GaAs quantum dot lasers on on-axis Si (001). Opt Express, 2019, 27: 2681–2688
87 Yang Y, Jiang J, Zeng J, et al. CH_4, C_2H_6, and CO_2 multi-gas sensing based on portable mid-infrared spectroscopy and PCA-BP algorithm. Sensors, 2023, 23: 1413
88 Lewicki R, Witinski M, Li B, et al. Spectroscopic benzene detection using a broadband monolithic DFB-QCL array. In: Proceedings of the Novel In-Plane Semiconductor Lasers XV, 2016. 241–247
89 Wang Z l, Chang J, Tian C W, et al. Two-component gas quartz-enhanced photoacoustic spectroscopy sensor based on time-division multiplexing of distributed-feedback laser driver current. Appl Opt, 2019, 58: 8479–8485
90 Jiang J, Wang Z, Han X, et al. Multi-gas detection in power transformer oil based on tunable diode laser absorption spectrum. IEEE Trans Dielect Electr Insul, 2019, 26: 153–161
91 Zou M, Sun L, Wang X. Multigas sensing based on wavelength modulation spectroscopy using frequency division multiplexing combined with time division multiplexing. IEEE Sens J, 2022, 22: 12930–12938
92 Li J, Luo J, Shi L, et al. Rayleigh backscattering-based simultaneous linewidth narrowing of a multi-wavelength DFB laser array with an arbitrary wavelength spacing. Opt Lett, 2023, 48: 6188–6191
93 Shi L, Luo J, Jiang L, et al. Narrow linewidth semiconductor multi-wavelength DFB laser array simultaneously self-injection locked to a single microring resonator. Opt Lett, 2023, 48: 1974–1977
94 Lan T, Cao Z, Huang L, et al. Ultra-narrow-linewidth DFB laser array based on dual-cavity feedback. Opt Express, 2022, 30: 14617–14628
95 Sun Y, Yuan B, Sun X, et al. DFB laser array based on four phase-shifted sampled Bragg gratings with precise wavelength control. Opt Lett, 2022, 47: 6237–6240
96 Chen S, Xiao R, Sun Z, et al. Continuously-tunable DFB laser array for methane gas detection. In: Proceedings of the Asia Communications and Photonics Conference, 2019. 1–3
97 Zhang Y, Zheng J, Zhang F, et al. Study on DFB semiconductor laser array integrated with grating reflector based on reconstruction-equivalent-chirp technique. Opt Express, 2015, 23: 2889–2894
98 Chen M, Shi Y, Xiao R, et al. Tunable DFB laser array for multi-gas detection. In: Proceedings of the 19th International Conference on Optical Communications and Networks, 2021. 1–3
99 Yuan W, Zhao J, Wang Y, et al. 10×10 Gbs directly modulated DFB laser array based on the REC technique. Appl Opt, 2023, 62: 5917–5920
100 Tang S, Hou L, Chen X, et al. Multiple-wavelength distributed-feedback laser arrays with high coupling coefficients and precise channel spacing. Opt Lett, 2017, 42: 1800–1803
101 Ma Y, Ge H, Sun Z, et al. High-power tapered two-section distributed feedback laser based on a chirped sampled grating. Appl Opt, 2023, 62: 2661–2668
102 Sun X, Li Z, Fan Y, et al. Multi-wavelength DFB laser based on a sidewall third-order four phase-shifted sampled Bragg grating with uniform wavelength spacing. Opt Lett, 2025, 50: 714–717
103 Karnik T S, Diehl L, Du Q, et al. On-chip wavelength beam combined DFB quantum cascade laser arrays. Opt Lett, 2025, 50: 2409–2412
104 Tao Y S, Tao Z H, Li L, et al. Silicon integrated microwave photonics. Sci China Inf Sci, 2025, 68: 140401
105 Mashanovich G Z, Stankovic S, Topley R, et al. Silicon photonic waveguides and devices for near- and Mid-IR applications. IEEE J Sel Top Quantum Electron, 2014, 21: 407–418
106 Zhao Y, Jang J K, Beals G J, et al. All-optical frequency division on-chip using a single laser. Nature, 2024, 627: 546–552
107 Ma Y, Chang Y, Dong B, et al. Heterogeneously integrated graphene/silicon/halide waveguide photodetectors toward chip-scale zero-bias long-wave infrared spectroscopic sensing. ACS Nano, 2021, 15: 10084–10094
108 Liu M, Yin X, Ulin-Avila E, et al. A graphene-based broadband optical modulator. Nature, 2011, 474: 64–67

109 Tian R, Gan X, Li C, et al. Chip-integrated van der Waals PN heterojunction photodetector with low dark current and high responsivity. Light Sci Appl, 2022, 11: 101
110 Rong K, Gan F, Shi K, et al. Configurable integration of on-chip quantum dot lasers and subwavelength plasmonic waveguides. Adv Mater, 2018, 30: e1706546
111 Ng K W, Ko W S, Tran T T D, et al. Unconventional growth mechanism for monolithic integration of III-V on silicon. ACS Nano, 2013, 7: 100–107
112 Bioud Y A, Boucherif A, Myronov M, et al. Uprooting defects to enable high-performance III-V optoelectronic devices on silicon. Nat Commun, 2019, 10: 4322
113 Wei W Q, Feng Q, Guo J J, et al. InAs/GaAs quantum dot narrow ridge lasers epitaxially grown on SOI substrates for silicon photonic integration. Opt Express, 2020, 28: 26555–26563
114 Wang Z, Tian B, Pantouvaki M, et al. Room-temperature InP distributed feedback laser array directly grown on silicon. Nat Photon, 2015, 9: 837–842
115 Vogelbacher F, Schotter J, Sagmeister M, et al. Integrated silicon nitride organic hybrid DFB laser with inkjet printed gain medium. Opt Express, 2019, 27: 29350–29356
116 Wang Y, Chen S, Yu Y, et al. Monolithic quantum-dot distributed feedback laser array on silicon. Optica, 2018, 5: 528–533
117 Hnida-Gut K E, Sousa M, Tiwari P, et al. Selective electrodeposition of indium microstructures on silicon and their conversion into InAs and InSb semiconductors. Discover Nano, 2023, 18: 4
118 Remis A, Monge-Bartolome L, Paparella M, et al. Unlocking the monolithic integration scenario: optical coupling between GaSb diode lasers epitaxially grown on patterned Si substrates and passive SiN waveguides. Light Sci Appl, 2023, 12: 150
119 Koscica R, Wan Y, He W, et al. Heterogeneous integration of a III-V quantum dot laser on high thermal conductivity silicon carbide. Opt Lett, 2023, 48: 2539–2542
120 Tanabe K, Watanabe K, Arakawa Y. III-V/Si hybrid photonic devices by direct fusion bonding. Sci Rep, 2012, 2: 349
121 Kishibe K, Hirata S, Inoue R, et al. Wavelength-conversion-material-mediated semiconductor wafer bonding for smart optoelectronic interconnects. Nanomaterials, 2019, 9: 1742
122 Burakowski M, Holewa P, Mrowiński P, et al. Heterogeneous integration of single InAs/InP quantum dots with the SOI chip using direct bonding. Opt Express, 2024, 32: 10874–10886
123 Ohira K, Kobayashi K, Iizuka N, et al. On-chip optical interconnection by using integrated III-V laser diode and photodetector with silicon waveguide. Opt Express, 2010, 18: 15440–15447
124 Wang R, Sprengel S, Boehm G, et al. Broad wavelength coverage 2.3 μm III-V-on-silicon DFB laser array. Optica, 2017, 4: 972–975
125 Stankovic S, Jones R, Sysak M N, et al. Hybrid III-V/Si distributed-feedback laser based on adhesive bonding. IEEE Photon Technol Lett, 2012, 24: 2155–2158
126 Keyvaninia S, Verstuyft S, van Landschoot L, et al. Heterogeneously integrated III-V/silicon distributed feedback lasers. Opt Lett, 2013, 38: 5434–5437
127 Thiessen T, Menezo S, Jany C, et al. Back-side-on-BOX heterogeneously integrated III-V-on-silicon O-band discrete-mode lasers. Opt Express, 2020, 28: 38579–38591
128 Chowdhury S J, Wickremasinghe K, Grist S M, et al. On-chip hybrid integration of swept frequency distributed-feedback laser with silicon photonic circuits using photonic wire bonding. Opt Express, 2024, 32: 3085–3099
129 Wen P, Tiwari P, Mauthe S, et al. Waveguide coupled III-V photodiodes monolithically integrated on Si. Nat Commun, 2022, 13: 909
130 Yang C, Liang L, Qin L, et al. Advances in silicon-based, integrated tunable semiconductor lasers. Nanophotonics, 2023, 12: 197–217
131 Yu Q, Gao J, Ye N, et al. Heterogeneous photodiodes on silicon nitride waveguides. Opt Express, 2020, 28: 14824–14830
132 Wang J, Long Y. On-chip silicon photonic signaling and processing: a review. Sci Bull, 2018, 63: 1267–1310
133 Kou R, Hiratani T, Yagi H, et al. Inter-layer light transition in hybrid III-V/Si waveguides integrated by μ-transfer printing. Opt Express, 2020, 28: 19772–19782
134 Zhang J, de Groote A, Abbasi A, et al. Silicon photonics fiber-to-the-home transceiver array based on transfer-printing-based integration of III-V photodetectors. Opt Express, 2017, 25: 14290–14299
135 Zhang J, Haq B, O'Callaghan J, et al. Transfer-printing-based integration of a III-V-on-silicon distributed feedback laser. Opt Express, 2018, 26: 8821–8830
136 Haq B, Rahimi Vaskasi J, Zhang J, et al. Micro-transfer-printed III-V-on-silicon C-band distributed feedback lasers. Opt Express, 2020, 28: 32793–32801
137 Kaushik V, Rajput S, Srivastav S, et al. On-chip nanophotonic broadband wavelength detector with 2D-electron gas. Nanophotonics, 2022, 11: 289–296
138 De Groote A, Cardile P, Subramanian A Z, et al. Transfer-printing-based integration of single-mode waveguide-coupled III-V-on-silicon broadband light emitters. Opt Express, 2016, 24: 13754–13762
139 Cuyvers S, Hermans A, Kiewiet M, et al. Heterogeneous integration of Si photodiodes on silicon nitride for near-visible light detection. Opt Lett, 2022, 47: 937–940
140 Goyvaerts J, Kumari S, Uvin S, et al. Transfer-print integration of GaAs p-i-n photodiodes onto silicon nitride waveguides for near-infrared applications. Opt Express, 2020, 28: 21275–21285
141 Wang D, Kannojia H K, Jouy P, et al. Innovative integration of dual quantum cascade lasers on silicon photonics platform. Micromachines, 2024, 15: 1055
142 Theurer M, Moehrle M, Sigmund A, et al. Flip-chip integration of InP to SiN photonic integrated circuits. J Lightwave Technol, 2020, 38: 2630–2636
143 Fujioka N, Chu T, Ishizaka M. Compact and low power consumption hybrid integrated wavelength tunable laser module using silicon waveguide resonators. J Lightwave Technol, 2010, 28: 3115–3120
144 Qiao S, He Y, Sun H, et al. Ultra-highly sensitive dual gases detection based on photoacoustic spectroscopy by exploiting a long-wave, high-power, wide-tunable, single-longitudinal-mode solid-state laser. Light Sci Appl, 2024, 13: 100
145 Liu Y Z, Yu M Y, Tan Y D, et al. Midinfrared cavity-enhanced two-photon absorption spectroscopy for selective detection of trace gases. Anal Chem, 2025, 97: 848–853
146 Pei W, Li H, Cui Y, et al. Narrow-linewidth 2 μm all-fiber laser amplifier with a highly stable and precisely tunable wavelength for gas molecule absorption in photonic crystal hollow-core fibers. Molecules, 2021, 26: 5323
147 Ji J, Wang H, Ma J, et al. Narrow linewidth self-injection locked fiber laser based on a crystalline resonator in add-drop configuration.

Opt Lett, 2022, 47: 1525–1528
148 Han M, Li J, Yu H, et al. Integrated self-injection-locked narrow linewidth laser based on thin-film lithium niobate. Opt Express, 2024, 32: 5632–5640
149 Duan L, Zhang H, Shi W, et al. High-resolution temperature sensor based on single-frequency ring fiber laser via optical heterodyne spectroscopy technology. Sensors, 2018, 18: 3245
150 Xu T, Geng Z, Su Y. A potential plasmonic biosensor based asymmetric metal ring cavity with extremely narrow linewidth and high sensitivity. Sensors, 2021, 21: 752
151 Riemensberger J, Lukashchuk A, Karpov M, et al. Massively parallel coherent laser ranging using a soliton microcomb. Nature, 2020, 581: 164–170
152 Li H, Zheng K, Ge R, et al. Noise-tolerant LiDAR approaching the standard quantum-limited precision. Light Sci Appl, 2025, 14: 138
153 Feng Z, Yang F, Zhang X, et al. Ultra-low noise optical injection locking amplifier with AOM-based coherent detection scheme. Sci Rep, 2018, 8: 13135
154 Cui Q, Lei Y X, Chen Y Y, et al. Advances in wide-tuning and narrow-linewidth external-cavity diode lasers. Sci China Inf Sci, 2022, 65: 181401
155 Aflatouni F, Hashemi H. Wideband tunable laser phase noise reduction using single sideband modulation in an electro-optical feed-forward scheme. Opt Lett, 2012, 37: 196–198
156 Lang X K, Jia P, Chen Y Y, et al. Advances in narrow linewidth diode lasers. Sci China Inf Sci, 2019, 62: 61401
157 Yang J, Jiang Z, Benthin F, et al. High-rate intercity quantum key distribution with a semiconductor single-photon source. Light Sci Appl, 2024, 13: 150
158 Ding X, He Y, Duan Z C, et al. On-demand single photons with high extraction efficiency and near-unity indistinguishability from a resonantly driven quantum dot in a micropillar. Phys Rev Lett, 2016, 116: 020401
159 Dusanowski Ł, Kwon S H, Schneider C, et al. Near-unity indistinguishability single photon source for large-scale integrated quantum optics. Phys Rev Lett, 2019, 122: 173602
160 Grange T, Somaschi N, Antón C, et al. Reducing phonon-induced decoherence in solid-state single-photon sources with cavity quantum electrodynamics. Phys Rev Lett, 2017, 118: 253602
161 Chen C, Yan J Y, Babin H G, et al. Wavelength-tunable high-fidelity entangled photon sources enabled by dual Stark effects. Nat Commun, 2024, 15: 5792
162 Davanco M, Liu J, Sapienza L, et al. Heterogeneous integration for on-chip quantum photonic circuits with single quantum dot devices. Nat Commun, 2017, 8: 889
163 Zhou Z, Ou X, Fang Y, et al. Prospects and applications of on-chip lasers. eLight, 2023, 3: 1
164 Wang R, Muneeb M, Sprengel S, et al. III-V-on-silicon 2-μm-wavelength-range wavelength demultiplexers with heterogeneously integrated InP-based type-II photodetectors. Opt Express, 2016, 24: 8480–8490
165 Green W M J, Zhang E J, Xiong C, et al. Silicon photonic gas sensing. In: Processing of the Optical Fiber Communication Conference, 2019
166 Meyer J R, Kim C S, Kim M, et al. Interband cascade photonic integrated circuits on native III-V chip. Sensors, 2021, 21: 599
167 Poulton C V, Yaacobi A, Cole D B, et al. Coherent solid-state LIDAR with silicon photonic optical phased arrays. Opt Lett, 2017, 42: 4091–4094
168 Yue J, Cui A, Wang F, et al. Design of monolithic 2D optical phased arrays heterogeneously integrated with on-chip laser arrays based on SOI photonic platform. Micromachines, 2022, 13: 2117
169 Zhang G, Haw J Y, Cai H, et al. An integrated silicon photonic chip platform for continuous-variable quantum key distribution. Nat Photonics, 2019, 13: 839–842
170 Wan Y, Zhang S, Norman J C, et al. Tunable quantum dot lasers grown directly on silicon. Optica, 2019, 6: 1394–1400
171 Ren M, Cai H, Chin L K, et al. Coupled-ring reflector in an external-cavity tunable laser. Optica, 2015, 2: 940–943
172 Pan B, Bourderionnet J, Billault V, et al. III-V-on-Si_3N_4 widely tunable narrow-linewidth laser based on micro-transfer printing. Photon Res, 2024, 12: 2508–2520
173 Xiang S Y, Gao S, Shi Y C, et al. Experimental demonstration of a photonic spiking neuron based on a DFB laser subject to side-mode optical pulse injection. Sci China Inf Sci, 2024, 67: 132402
174 García-Meca C, Lechago S, Brimont A, et al. On-chip wireless silicon photonics: from reconfigurable interconnects to lab-on-chip devices. Light Sci Appl, 2017, 6: e17053
175 Farmakidis N, Youngblood N, Li X, et al. Plasmonic nanogap enhanced phase-change devices with dual electrical-optical functionality. Sci Adv, 2019, 5: eaaw2687
176 Yang J, Tang M, Chen S, et al. From past to future: on-chip laser sources for photonic integrated circuits. Light Sci Appl, 2023, 12: 16
177 Maskoun J, Gheshlaghi N, Isik F, et al. Optical microfluidic waveguides and solution lasers of colloidal semiconductor quantum wells. Adv Mater, 2021, 33: e2007131
178 Chen Y F, Yu J J, Wang C, et al. Cost-effective 200-Gbps/λ coherent PON enabled by DFB lasers and a pilot-based carrier recovery. Sci China Inf Sci, 2025, 68: 179301
179 Low L A, Mummery C, Berridge B R, et al. Organs-on-chips: into the next decade. Nat Rev Drug Discov, 2021, 20: 345–361